

UNIVERSIDADE FEDERAL DO ESPÍRITO SANTO (UFES)
CENTRO TECNOLÓGICO
PROGRAMA DE PÓS-GRADUAÇÃO EM ENGENHARIA CIVIL

JULIA AMARAL RODRIGUES

**CRACK MODELING OF ASPHALT MIXTURES USING NONLINEAR
VISCOELASTIC COHESIVE ZONE (NVCZ) TO ASSESS THE INFLUENCE OF
DIFFERENT FILLERS IN THE MATERIAL'S FRACTURE RESISTANCE**

VITÓRIA

2018

JULIA AMARAL RODRIGUES

**CRACK MODELING OF ASPHALT MIXTURES USING NONLINEAR
VISCOELASTIC COHESIVE ZONE (NVCZ) TO ASSESS THE INFLUENCE OF
DIFFERENT FILLERS IN THE MATERIAL'S FRACTURE RESISTANCE**

A Thesis submitted as a partial fulfillment of the requirements for the Master's Degree in Civil Engineering at Universidade Federal do Espírito Santo.

Advisor: Jamilla Emi Sudo Lutif Teixeira, Ph.D.

VITÓRIA

2018

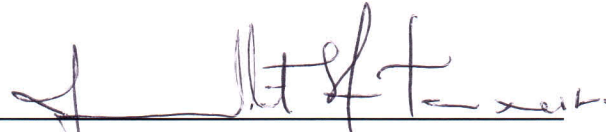
UNIVERSIDADE FEDERAL DO ESPÍRITO SANTO

CRACK MODELING OF ASPHALT MIXTURES USING NONLINEAR VISCOELASTIC COHESIVE ZONE (NVCZ) TO ASSESS THE INFLUENCE OF DIFFERENT FILLERS IN THE MATERIAL'S FRACTURE RESISTANCE

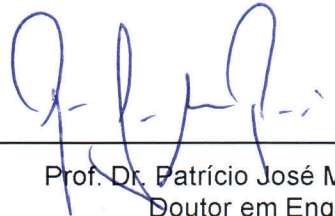
Julia Amaral Rodrigues

Dissertação apresentada ao Curso de Mestrado em Engenharia Civil do Programa de Pós-Graduação em Engenharia Civil da Universidade Federal do Espírito, como requisito parcial para obtenção do título de Mestre em Engenharia Civil, área de Construção Civil.

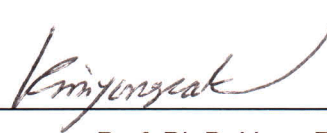
Aprovada no dia **22 de agosto de 2018** por:



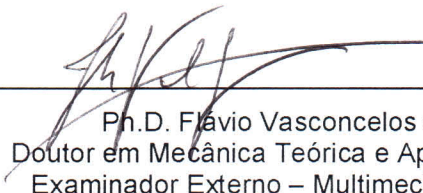
Prof. Ph. D. Jamilla Emi Sudo Lutif Teixeira
Doutora em Engenharia Civil
Orientadora – UFES



Prof. Dr. Patrício José Moreira Pires
Doutor em Engenharia Civil
Examinador Interno - UFES



Prof. Ph.D. Yong-Rak Kim
Doutor em Engenharia Civil
Examinador Externo – UNL (EUA)



Ph.D. Flávio Vasconcelos Souza
Doutor em Mecânica Teórica e Aplicada
Examinador Externo – Multimechanics

Vitória – ES, agosto de 2018

Dados Internacionais de Catalogação-na-publicação (CIP)
(Biblioteca Setorial Tecnológica,
Universidade Federal do Espírito Santo, ES, Brasil)

R696c Rodrigues, Julia Amaral, 1991-
Crack modeling of asphalt mixtures using nonlinear viscoelastic cohesive zone (NVCZ) to assess the influence of different fillers in the material's fracture resistance / Julia Amaral Rodrigues. – 2018.
95 f. : il.

Orientador: Jamilla Emi Sudo Lutf Teixeira.
Dissertação (Mestrado em Engenharia Civil) – Universidade Federal do Espírito Santo, Centro Tecnológico.

1. Materiais betuminosos. 2. Pavimentos de asfalto.
3. Mecânica da fratura. 4. Viscoelasticidade. 5. Modelagem numérica. 6. Zona Coesiva. I. Teixeira, Jamilla Emi Sudo Lutf.
II. Universidade Federal do Espírito Santo. Centro Tecnológico.
III. Título.

CDU: 624

ABSTRACT

Micromechanical numerical models have become an important tool in the study of asphaltic pavements given its numerous advantages in comparison to analytical, semi-empirical and/or completely experimental approaches. Thus, this study presents a framework to predict the behavior of bituminous composites considering viscoelasticity and fracture resistance based on nonlinear viscoelastic cohesive zone (NVCZ) model. The NVCZ model is able to predict the entire fracture process, from crack nucleation, initiation, and propagation in mixture microstructure. To examine the NVCZ model, two fine aggregate matrix (FAM) mixtures containing different fillers (hydrated lime and steel slag) were evaluated experimentally and compared to the numerical results. FAM material linear-viscoelastic properties and fracture parameters required as input for the numerical modelling were experimentally obtained. Linear-viscoelastic properties were obtained by performing frequency sweep tests and the required NVCZ parameters were obtained by an experimental-numerical calibration procedure using semi-circular bending (SCB) laboratory tests coupled with finite element numerical simulations. To validate the model, microstructural numerical simulations of the indirect tensile strength test (IDT) were conducted and compared to experimental results. Numerical modeling results agree well with laboratory testing results. The results of this research imply that the NVCZ model is promising to evaluate the cohesive fracture resistance of different material constituents in bituminous composites with significant savings in experimental costs and time.

Keywords: Bituminous materials, Fracture, Viscoelasticity, Cohesive Zone

RESUMO

Modelos numéricos micromecânicos tornaram-se uma ferramenta importante para previsão do comportamento de compósitos, dadas as suas inúmeras vantagens em comparação com abordagens analíticas, semi-empíricas e/ou totalmente experimentais. Desta forma, este estudo apresenta um modelo numérico computacional para prever o comportamento de compósitos betuminosos considerando seu comportamento viscoelástico e resistência à fratura com base em modelo de zona coesiva viscoelástica não linear (ZCNV). O modelo ZCNV é capaz de prever todo o processo de fratura, desde a nucleação, iniciação e propagação da trinca na microestrutura da mistura asfáltica. Para validar o modelo, duas misturas de MAF (matriz asfáltica de finos) contendo diferentes fillers (cal hidratada e escória de aciaria) foram avaliadas experimentalmente e os resultados experimentais comparados com os resultados numéricos. As propriedades viscoelásticas lineares das MAF's e os parâmetros de fratura necessários para a modelagem numérica foram obtidos experimentalmente. As propriedades viscoelásticas lineares foram obtidas através da realização de testes de varredura de frequência e os parâmetros de fratura requeridos foram obtidos por um procedimento de calibração numérica experimental usando testes de laboratório de flexão semicircular (SCB) acoplados a simulações numéricas de elementos finitos. Para validar o modelo, foram realizados ensaios laboratoriais de tração indireta (TI) e os resultados foram comparados com resultados numéricos para o mesmo ensaio com as mesmas condições de contorno. Os resultados da modelagem numérica foram compatíveis com os resultados dos testes laboratoriais. Os resultados desta pesquisa implicam que o modelo ZCNV é eficiente para avaliar a influência da adição de diferentes materiais em matrizes asfálticas com relação a resistência à fratura sendo, portanto, uma importante ferramenta para auxiliar na análise da influência de materiais no comportamento de misturas asfálticas, trazendo economias significativas em custo e tempo.

Palavras-chave: Materiais betuminosos, Fratura, Viscoelasticidade, Zona Coesiva

DEDICATION

*To my family,
for always believing in me and supporting me in all my choices.*

ACKNOWLEDGEMENTS

First of all, I would like to express my deepest sincere gratitude to my excellent adviser, professor Jamilla Emi Sudo Lutf Teixeira, who is the main responsible for all the work I have done. I am very grateful to her for having believed in my potential since my first day of my master's graduate program. I thank her for the opportunities she has given me, and her unconditional support, teachings, advices and her extreme dedication in my career and research. I also want to publicly thank her for having encouraged me to face challenges that I did not imagine I would be capable of.

I thank my family, parents, brother, sister-in-law and aunts for always being present in my life and encouraging me to always give my best.

I express my sincere gratitude to professors Yong-Rak Kim, Flavio Souza, and Patrício Pires for accepting the invitation in being the committee members of my master thesis defense and contributions to improve the research developed.

I would like to thank the company MultiMechanics, for freely extending the license period which was essential to complete this research. Also, I thank the company support team, especially Hayden Cornwell, who gave me the support I needed while using the software.

I also would like to thank Victor Ferreira Teixeira who helped me with his knowledge and experience with numerical modeling.

Thanks to the technicians of Laboratório de Ensaios em Materiais de Construção (LEMAC) and Laboratório de Mecânica dos Solos (LAMES) of UFES for all the dedication and experience shared during my experimental tests.

I thank my colleagues who I have won during the master's graduate program, and those who have come with me since undergraduate studies. During this period together we share doubts, anguish and valuable learning.

Finally, I would like to thank the professors and collaborators of the Graduate Program in Civil Engineering (PPGEC) of UFES, for the transmitted knowledge and availability.

GRANT INFORMATION

I would like to acknowledge the scholarship financial support provided by the *Coordenação de Aperfeiçoamento de Pessoal de Nível Superior (CAPES)*.

Also, I would like to thank the *Fundação de Amparo à Pesquisa e Inovação do Espírito Santo (FAPES)* for the financial support in the project entitled: *Avaliação Numérica e Experimental de Propriedades de Concretos produzidos com Rejeitos Industriais*. Projeto Universal Individual de Pesquisa - TO: 0506/2015, enabling the purchase of MultiMech software license used in this research.

Finally, I would like to acknowledge the *Conselho Nacional de Desenvolvimento Científico e Tecnológico (CNPQ)* for financial support in the project entitled: *Modelagem Numérica Multi-Escala para Avaliação do Comportamento Mecânico de Concretos Asfálticos considerando Dano associado à Viscoelasticidade e ao Crescimento e Propagação de Trincas*. CNPQ Chamada Universal –MCTI/CNPq No 14/2014 Faixa A, which resulted in this master thesis work.

LIST OF FIGURES

FIGURE 1-PAVEMENT CLASSIFICATION - CNT SURVEY.....	17
FIGURE 2 - (A) MACROCRACKS FORMED DUE TO EXCESSIVE FATIGUE CRACKING (B) PERMANENT DEFORMATION.....	18
FIGURE 3-ILLUSTRATION OF MACROCRACKS FORMATION DUE TO MICROCRACKS IN DIFFERENT LENGTH SCALES.....	19
FIGURE 4 – DAMAGE AND EFFECTIVE UNDAMAGED CONFIGURATIONS.....	25
FIGURE 5 - SCHEMATIC REPRESENTATION OF MICROSTRUCTURE MODEL INITIAL BOUNDARY VALUE PROBLEM.	27
FIGURE 6 - SCHEMATIC ILLUSTRATION OF COHESIVE ZONE MODELING CONCEPT.....	29
FIGURE 7- EXAMPLES OF SOFTENING FUNCTIONS OF CZM PROPOSED IN THE LITERATURE.	30
FIGURE 8 - A FINITE ELEMENT MESH AND ITS BOUNDARY CONDITIONS TO MODEL THE SCB TESTING.....	31
FIGURE 9 - ILLUSTRATION OF THE SCB SPECIMEN WITH ITS MATERIAL PROPERTIES THE LINEARLY DECAYING MIXED-MODE COHESIVE ZONE MODEL.....	32
FIGURE 10 - SCHEMATIC ILLUSTRATION OF STEEL PRODUCTION BY THREE DIFFERENT ROUTES.	36
FIGURE 11-SCHEMATIC ILLUSTRATION OF BOF E EAF.	37
FIGURE 12 - SCHEMATIC ILLUSTRATION OF RESEARCH METHODOLOGY.	40
FIGURE 13 - GRADATION CURVES OF AGGREGATES.....	42
FIGURE 14 - MINERALOGICAL CHARACTERISTICS OF HYDRATED LIME PARTICLES.....	43
FIGURE 15-MINERALOGICAL CHARACTERISTICS OF LD STEEL SLAG PARTICLES.	44
FIGURE 16- GRADATION CURVES OF THE FINE AGGREGATE MATRIX AND THE COMPLETE BITUMINOUS COMPOSITE.	45

FIGURE 17 - FAM SAMPLE FABRICATION PROCESS: (A) FAM MIXTURE BATCH); ((B) SAMPLE MOLD; (C) MIXTURE BEING PLACED IN THE MOLD; (D) SAMPLE COMPACTION; (E) FAM DSR TESTING SAMPLE.....	47
FIGURE 18 - FREQUENCY SWEEP TEST RESULTS - FAM_HL.....	48
FIGURE 19 - FREQUENCY SWEEP TEST RESULTS - FAM_SS	48
FIGURE 20- MASTER CURVE OF DYNAMIC SHEAR MODULUS FOR THE ASPHALT MATRIX AT 25 °C.	49
FIGURE 21 - CURVES OF EXPERIMENTAL AND FITTED STORAGE MODULUS (G'), FAM_HL.....	51
FIGURE 22 - CURVES OF EXPERIMENTAL AND FITTED STORAGE MODULUS (G'), FAM_SS.....	51
FIGURE 23 - CALIBRATION PROCESS TO DETERMINE MODE I FRACTURE PARAMETERS.....	53
FIGURE 24-ILLUSTRATION OF SCB SPECIMEN CORING AND CUTTING PROCEDURE.	54
FIGURE 25 – ACTUAL SCB SPECIMEN CORING AND CUTTING PROCEDURE.....	54
FIGURE 26 - SCB TEST SET-UP.....	55
FIGURE 27 - LABORATORY RESULTS FOR SCB BENDING TESTS.	55
FIGURE 28 – ILLUSTRATION OF SCB MESHING REFINEMENT.....	56
FIGURE 29 – SCB MESH CONVERGENCE STUDY - SIMULATION RESULTS – MÁX. FORCE X ELEMENT SIZE.....	57
FIGURE 30 - δn * CALIBRANTION FOR (A) FAM_HL (B) FAM_SS.....	58
FIGURE 31 - m CALIBRANTION FOR (A) FAM_HL (B)FAM_SS.....	59
FIGURE 32 - A CALIBRANTION FOR (A) FAM_HL (B) FAM_SS.....	60
FIGURE 33 - σf CALIBRATION FOR (A) FAM_HL (B)FAM_SS.....	61
FIGURE 34 – MODE I FRACTURE PARAMETER AFTER CALIBRATION.	62
.FIGURE 35 – (A) IDT SAMPLE SETUP. (B) FAM_HL AND (C) FAM_SS AFTER TEST.	65
FIGURE 36 - LABORATORY RESULTS FOR IDT STRENGTH.....	66

FIGURE 37 - ELASTIC TAPER BAR PROBLEM.....	67
FIGURE 38 – TAPERED-BAR MESH CONVERGENCE STUDY FOR FOUR MESH REFINEMENT ELEMENT NUMBER: (A) 80 ELEMENTS; (B) 240 ELEMENTS; (C) 960 ELEMENTS; (D) 3000 ELEMENTS..	68
FIGURE 39 – TAPERED BAR MESH CONVERGENCE STUDY - MULTIMECH SIMULATION RESULTS.	68
FIGURE 40 - SCHEMATIC ILLUSTRATION AND RESULTS OF TAPERED BAR STRESS.	69
FIGURE 41-VISCOELASTIC TAPERED BAR PROBLEM.	70
FIGURE 42 - STRESS VALUES FROM ANALYTICAL AND MULTIMECH ANALYSIS AT THE POINT (0, 1) ON THE TAPERED BAR.	72
FIGURE 43 - SCHEMATIC ILLUSTRATION OF METHODOLOGY EMPLOYED FOR MODEL VALIDATION.	73
FIGURE 44 – IDT STRENGTH TEST MESH CONVERGENCE STUDY FOR COHESIVE ELEMENT SIZES.	74
FIGURE 45 – IDT MAX. REACTION FORCE VS. NUMBER OF ELEMENTS.	74
FIGURE 46 - TEST RESULTS VS. MICROSTRUCTURE MODEL SIMULATION RESULTS OF FAM BITUMINOUS MIXTURE: IDT VALIDATION.....	75
FIGURE 47 - DEFORMED MESH AND LONGITUDINAL STRESS CONTOURS BEFORE MICROCRACKING INITIATION AT DIFFERENT LOADING TIMES.	78
FIGURE 48 - DEFORMED MESH AND LONGITUDINAL STRESS CONTOURS AFTER MICROCRACKING INITIATION UNTIL COMPLETE FAILURE AT DIFFERENT LOADING TIMES.	79

LIST OF TABLES

TABLE 1 - CHEMICAL COMPOSITION OF BOF SLAG FROM MANY RESEARCHERS.....	37
TABLE 2 - ASPHALT BINDER CHARACTERIZATION.....	41
TABLE 3 - PHYSICAL CHARACTERISTICS OF THE AGGREGATES.	42
TABLE 4 - SEMI-QUANTITATIVE ANALYSIS IN THE FORM OF OXIDES OF THE STEEL SLAG BY FRX.	44
TABLE 5 - VOLUMETRIC PARAMETERS OF TESTING SAMPLES.....	47
TABLE 6 - PRONY SERIES COEFFICIENTS OF THE MATRIX PHASE AT 25°C.....	50
TABLE 7 - VOLUMETRIC PARAMETERS OF SCB TESTING SAMPLES.....	53
TABLE 8 - FRACTURE PARAMETERS USED FOR MESH CONVERGENCE STUDY.....	56
TABLE 9 – LVE MATERIAL PROPERTIES (PRONY SERIES) AND NLVE-CZM FRACTURE DAMAGE PARAMETERS FOR MODEL SIMULATIONS.....	62
TABLE 10 - MARSHALL TESTING SAMPLES VOLUMETRIC PARAMETERS FOR IDT TESTS.	65
TABLE 11- MATERIAL PROPERTIES FOR THE ELASTIC TAPERED BAR USED FOR THE ELASTIC MODEL VERIFICATION.....	67
TABLE 12- MATERIAL PROPERTIES USED FOR VISCOELASTIC VERIFICATION.	71
TABLE 13 – STRESS VALUES FROM ANALYTICAL AND MULTIMECH ANALYSIS.	71

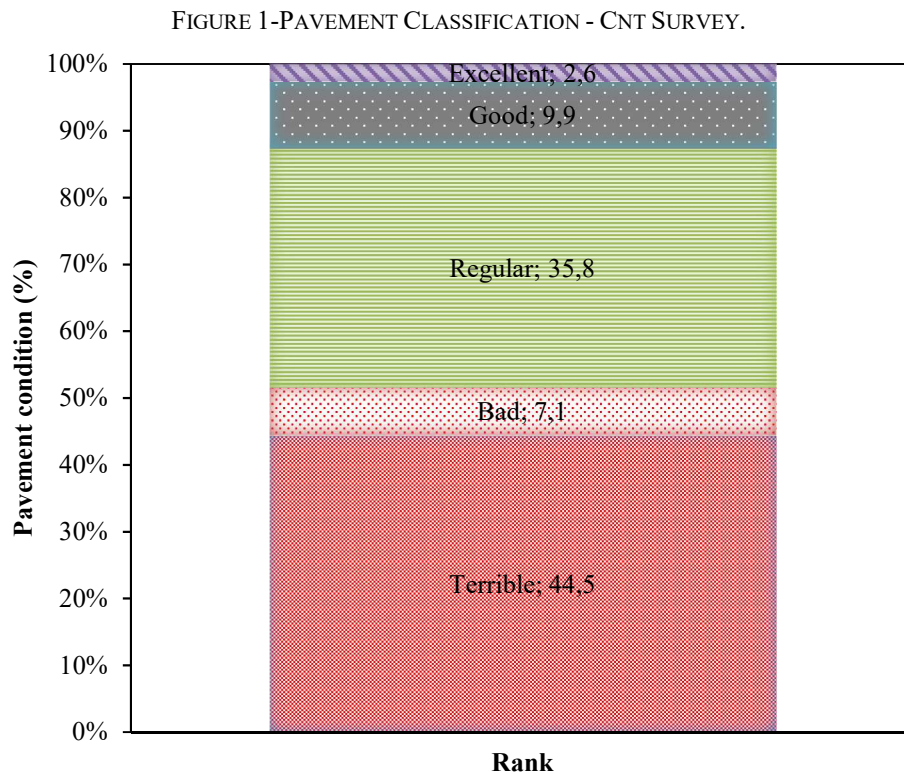
CONTENTS

1. INTRODUCTION	17
1.2 RESEARCH PROBLEM	20
1.3 RESEARCH OBJECTIVES	21
1.4 DISSERTATION LAYOUT	22
2. THEORETICAL BACKGROUND	24
2.1 CONTINUUM DAMAGE MODELING	25
2.2 MICROSTRUCTURE MODELS WITH DISCRETE FRACTURE	26
2.3. COHESIVE ZONE MODELS (CZM).....	29
2.4 USE OF LD STEEL SLAG AS FILLER IN ASPHALTIC MATERIALS	35
3. EXPERIMENTAL PROGRAM	40
3.1 MATERIAL CHARACTERIZATION	41
3.1.1 Asphalt binder	41
3.1.2 Aggregates	42
3.1.3 Fillers	42
3.2 FAM MIX DESIGN	45
3.3 LINEAR VISCOELASTIC PROPERTIES OF FAM_SS AND FAM_HL	46
3.3.1. DSR sample fabrication.....	46
3.3.2 FAM Linear Viscoelastic Properties	47
3.4 FRACTURE PROPERTIES OF FAM FAM_SS AND FAM_HL	51
3.4.1 SCB sample fabrication.....	53
3.4.2 SCB experimental test and numerical calibration using MultiMech TM software....	54
3.5 INDIRECT TENSION STRENGTH TEST (IDT)	63
3.5.1 IDT experimental setup and results.....	65
4. VERIFICATION AND VALIDATION OF MICROSTRUCTURE NUMERICAL MODEL	66
4.1 VERIFICATION OF ELASTIC CONSTITUTIVE MODELS WITHOUT DAMAGE.....	66
4.2 VERIFICATION OF VISCOELASTIC CONSTITUTIVE MODEL WITHOUT DAMAGE.....	70
4.3 VALIDATION OF THE MICROSTRUCTURE MODEL CONSIDERING DAMAGE	72
4.3.1 Mesh Convergence Study for IDT Strength Test Validation	73
4.3.2. Validation of IDT Strength Test with Damage	74

5. CONCLUDING REMARKS.....	81
FUTURE RESEARCH WORK	84
REFERENCES	85

1. INTRODUCTION

The transportation system plays an important role in the Brazilian economy, since the principal manner to transport people and goods are by roadways. The Brazilian highway network is about 1.7 million kilometers according to the latest report of National Confederation of Transport (CNT, 2015). From that total, 12.2% are considered paved, being 48.3% of paved roads ranked as in very poor conditions, as illustrated in Figure 1. Roadway users expect to have secure and comfortable pavement conditions while driving. For that, a minimum level of pavement distresses is desirable, i.e., minimum occurrences of permanent deformation, fatigue cracking, raveling, stripping and other are essential.



SOURCE: ADAPTED FROM CNT (2015).

The effects of traffic loads (whose volume increase along the years) and severe weather conditions, leads to the gradual degradation of pavement layers. In general, these distresses begin before the pavement reaches its design life. Among the main pavement

distresses, fatigue cracking and permanent deformation (Figure 2) are the principal causes of pavement's premature failure and rupture.

FIGURE 2 - (A) MACROCRACKS FORMED DUE TO EXCESSIVE FATIGUE CRACKING (B) PERMANENT DEFORMATION.



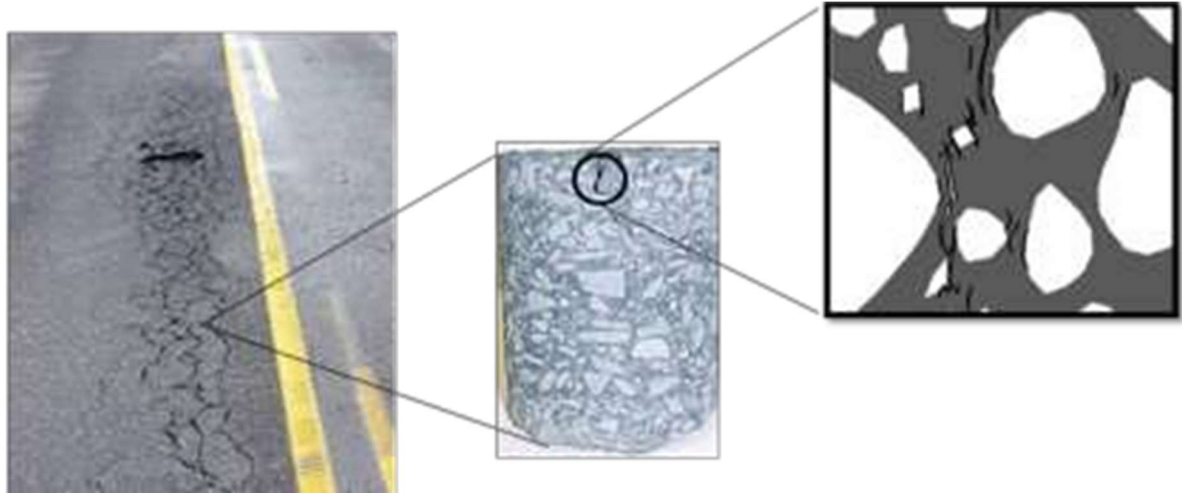
SOURCE: BERNUCCI ET AL. (2006).

Hot mix asphalt (HMA) is the main type of surface layer material used in Brazilian roadways and it is a composite material made by combining coarse and fine aggregates, asphalt binder, voids and oftentimes additives (natural filler, hydrated lime, polymers, etc). Due to the great differences in the constitutive behavior of each material constituent, individual characterization is essential to understand the overall HMA performance.

It is also worth mentioning that the large damage areas observed on the pavement surface are strongly related to the small-scale interaction that occurs when the pavement is subjected to different loading and climate conditions. As illustrated by Lutfi (2011) in Figure 3, the macroscale pavement cracking is a result of microcracking phenomena that begins in small scale of analysis, such as within the fine aggregate matrix (FAM) and/or in the interface of FAM or mastic and aggregates. Since FAM's performance is directly related to microcracking development, FAM characteristics should be carefully evaluated for better prediction of overall HMA performance. Different authors have been using FAM phase in their analysis and correlate its behavior with mixture level performance (KIM, 2003;

CASTELO BRANCO, 2008; KARKI, 2010; COUTINHO, 2012; UNDERWOOD and KIM, 2013; FONSECA, 2016; FREIRE et al. 2017 among others).

FIGURE 3-ILLUSTRATION OF MACROCRACKS FORMATION DUE TO MICROCRACKS IN DIFFERENT LENGTH SCALES.



SOURCE: LUTIF (2011).

Regarding the materials used in HMA composition, several studies have been developed to find more sustainable materials for pavement use. One important research line is about incorporation of waste or by-product materials into different phases of bituminous mixtures. Some by-products in fact, when added in bituminous composition, can improve mixture's performance due to positive changes in mixture's characteristics. Therefore, economic and environmental advantages are obtained, giving a commercial use to a valueless material and reducing natural resources exploration.

Steel industry utilize lots of slag former (lime and dolomite) during the steel production. From that process, different types of by-products are generated in form of slags, sludges, dusts, mill scales, etc. One of them is the steel slag, which comes from hot metal refining process using basic oxygen furnace (Linz-Donawitz converter) or electric arc furnace (DIAO et al., 2016). Slag generated from basic oxygen converter are usually refer as LD slag. Depending on the grade of steel produced, around 100–160 kg per ton of LD slag are generated (MAHIEUX *et al.*, 2008). The Brazilian LD slag generation in 2016 was about 2.4 – 4.8 Mt, being 0.56-1.16 Mt from the state of ES alone.

The LD slag reuse is still limited and undervalued. Various efforts have been made on the utilization of LD steel slags, such as in cement production (TSAKIRDIS, 2007; MONSHI et al., 1999), fertilizer production, road construction (CASTELO BRANCO, 2004; MAHIEUX, 2008; COSME et al., 2016; GOTTARDI, 2015; FONSECA, 2016), and so on. Regarding the roadway application, studies have shown that LD slag as aggregate provides better interlock in comparison with limestone aggregates (QAZIZADEH et al., 2018; ZIAEE et al., 2015). However, the slag volumetric expansion and its swelling due to its high content of free lime is still a major constraint to the application of that by-product in paving. More research efforts are necessary to verify the effects LD slag characteristic on asphalt mixture's performance.

1.2 RESEARCH PROBLEM

Most studies that aim to understand and/or to predict the asphaltic concrete behavior use semi-empirical methods or phenomenological techniques, relying on extensive and costly laboratory tests. Moreover, most of the procedures do not provide a clear effect of individual material's phase in the mixture global performance.

There is a need to evaluate the global behavior of asphalt concrete considering the fundamental properties of its constituents and their interactions. Even though there are many advances regarding experimental and numerical techniques to determine bituminous material's performance, still, an explicit way to identify damage initiation and propagation that occurs at small scales are necessary. The effects of new materials used for paving application in small scale needs to be carefully addressed. From the presented research statement problem, some research questions can be mentioned:

- Can LD steel slag be used as filler in asphalt mixture?
- What are the changes in overall material characteristics if LD slags are incorporated in HMA?
- Does the type of filler influence the speed of crack initiation and propagation?
- What are the limitations of using numerical modeling to predict mechanical behavior of asphalt concrete?
- What parameters and laboratory tests are needed to allow the use of numerical models?

1.3 RESEARCH OBJECTIVES

The primary goal of this research study is to model cracks in fine aggregate matrix (FAM) considering viscoelasticity and discrete fracture mechanisms. For that, a nonlinear viscoelastic cohesive zone model was used. Using this modelling technique, it is intended to evaluate the effects of LD steel slag on FAM viscoelasticity and fracture parameters.

Specific objectives of this research are:

1. Obtain linear viscoelastic material properties (LVE) experimentally by performing Frequency Sweep Tests on the studied FAM mixtures and compare the effects of different fillers (steel slag and hydrated lime) on FAM stiffness characteristics;
2. Obtain fracture parameters for the NVCZ model used herein based on experimental-numerical integrated approach by performing laboratory Semi-Circular Bending (SCB) tests and use this test as a step to numerically calibrate fracture parameters of studied FAM's.

3. Perform a parametric analysis of fracture parameters to identify the physical/mechanical effects of each mode parameters on FAM fracture resistance;
4. Verify the effect of different fillers in fracture characteristics of the studied FAM materials;
5. Validate the nonlinear viscoelastic cohesive zone model (NLVE-CZ) numerical model to predict the damage-dependent behavior of laboratory-fabricated bituminous mixture by comparing indirect tension tests results obtained numerically and experimentally;

1.4 DISSERTATION LAYOUT

Following this introductory chapter, *Chapter 2* is dedicated to a literature review on several approaches attempting to predict the mechanical behavior of bituminous composites, as well as advantages, limitations, and shortcomings of these approaches. In addition, a review on the by-product used as a potential substitute for the filler hydrated lime in asphalt mixtures as presented, containing its production process and its main characteristics that make it an attractive application material in asphalt paving. In *Chapter 3* describes the experimental testing program designed in this research to obtain material properties of the FAM mixture phases required for the model validation, besides that, the chapter contains the numerical simulations and results to determine viscoelastic properties of FAM and calibration process to determine cohesive zone fractures parameters. It also shows all the characterization of the materials used during the research on the asphalt mixture and FAM mix design. Details about bituminous composite specimen geometry and material properties, as well as the loading conditions used in the indirect tensile strength tests for model validation, that are used in later chapter (*Chapter 4*), are shown. *Chapter 4* consists of several approaches attempting to validation the model and the validation-calibration of the model to predict damage-dependent behavior of laboratory fabricated asphaltic composites. Comparisons of experimental results from indirect tensile strength tests with numerical results are presented. *Chapter 5* presents

the conclusions of the research and recommendations for future work required to improve the model predictions.

2. THEORETICAL BACKGROUND

Pavement structures are subjected to large number of solicitations over time, such as repetitive traffic loading, temperature gradients, rain and/or snow conditions, etc. The effect of those solicitations is the reduction of pavement performance due to the occurrence of different types of distresses, such as plastic deformation (rutting), loss of adhesion (raveling and stripping), formation of cracks (longitudinal and/or transverse cracks), potholes, etc. Most of those distresses are result of crack initiation and propagation within the asphalt media. Thus, it is important to understand how this damage starts and what factors can accelerate its propagation.

Numerous studies have been carried out over the past decades to obtain a better understanding of asphalt concrete fracture mechanisms and, thus, to address the cracking problem in asphalt pavements. The composite material performance depends directly on the selection and proportion of the constituents used in the mixture design and the interactions to each other. Methodologies are needed to provide the designer with as much information as possible about the microstructure behavior and the influence of each constituent in the behavior of the mixture. Given all the complexity to predict the behavior of asphalt materials (which include material anisotropy, damage in different length scales, viscoelasticity, aging, etc.), many scientific investigations are developed to reach at more efficient and precise methods of analyzing the behavior of these materials.

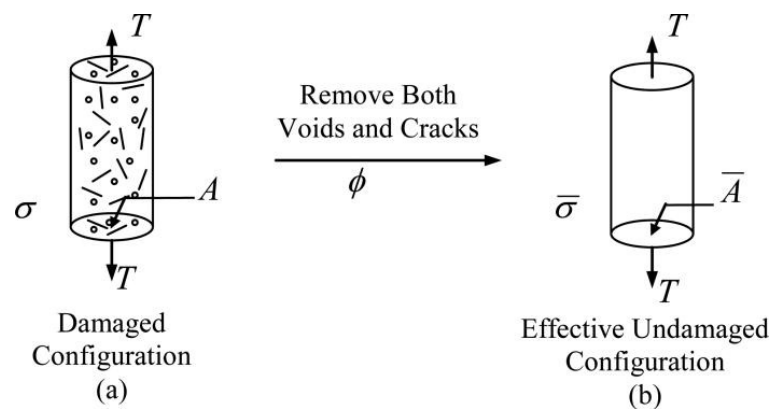
One methodology that has been widely used in the scientific community is numerical modeling. With the advances in computer power, and in numerical techniques, the prediction of material's behavior based on virtual observations is a reality that could overcome many uncertainties obtained when only experimental analysis is performed. Among the most studied numerical approaches to study composite materials, two modeling techniques are

highlighted by the pavement community: (i) continuous damage-based models and (ii) microstructural models. The use of each of these models has advantages, although they also have their limitations.

2.1 CONTINUUM DAMAGE MODELING

In such models, asphalt composites are treated as homogenous bodies, and the state of damage is quantified in a homogenized way without performing microstructure analysis, using phenomenological internal state variables (ISVs). Thus, ISVs quantify the material internal damages (micro-cracks, chemical variations, etc.). Then, no internal contour (discrete cracks) is considered, and the internal variables are the only ones responsible for quantifying the energy dissipation caused by the propagation of cracks. The crack formation and propagation are not explicitly considered. Figure 4 presents the concept of effective stress for the case of uniaxial tension introduced by Kachanov (1958) and Rabotnov (1969) in continuum damage mechanics models. In this case the effective stress $\bar{\sigma}$ is the stress applied to a fictitious state of the material which is totally undamaged. This fictitious state is assumed to be mechanically equivalent to the actual damaged state of the material (VOYIADJIS AND KATTAN, 2012).

FIGURE 4 – DAMAGE AND EFFECTIVE UNDAMAGED CONFIGURATIONS.



SOURCE: VOYIADJIS AND KATTAN (2012).

Since the cracks in microscales are not modeled explicitly there is a great saving in computational time, which makes the model attractive. Several authors have used this model given this advantage (SCHAPERLY, 1990; PARK et al., 1996; LEE and KIM, 1998; CHEHAB et al. 2002; DANIEL and KIM, 2002; BERTHELOT et al. 2003; TEIXEIRA et al., 2007).

The main disadvantage of continuum damage models is the definition of the laws of damage evolution that govern the ISVs. They are determined through regression analyses by matching damage evolution characteristics from laboratory testing observations. These are a somewhat arbitrary choice and requires a large number of experimental tests.. Still, according to Caiazzo and Costanzo (2001), these laws are insufficient to know the cause and evolution of the damage.

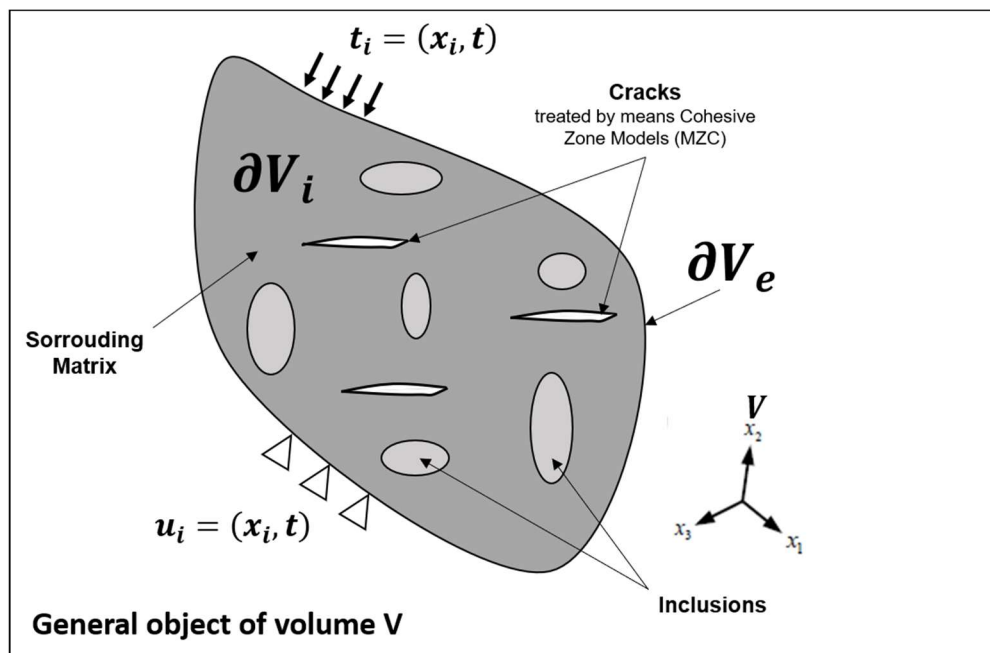
2.2 MICROSTRUCTURE MODELS WITH DISCRETE FRACTURE

Micromechanical models take into account the heterogeneity of the composite materials, considering the properties and behavior of each constituent, as well as the interactions between them. Then, the effective properties of composite materials are determined from known properties of each constituent of the composite. Among main advantages of computational microstructure models, over other methods such as continuum damage approach, is that once the properties of the constituents have been determined, the resulting properties of the composite can be determined computationally for different types of material's proportions, without requiring a large number of time-consuming laboratory tests for each of them.

To better understand the microstructure modelling approach, the first step is to describe the problem. Figure 5 represent to the initial boundary value problem (IBVP) for a

general elastic-viscoelastic composite containing cracks. Consider an object of volume V and a boundary ∂V which is divided into two parts, ∂V_e (external boundary) and ∂V_i (internal boundary with cohesive zones). There are three variables predicted by the model, they are: the displacement vector $u_i(x_m, t)$, the stress tensor $\sigma_{ij}(x_m, t)$, and the strain tensor $\varepsilon_{ij}(x_m, t)$, where t and x_m are time and spatial coordinate, respectively.

FIGURE 5 - SCHEMATIC REPRESENTATION OF MICROSTRUCTURE MODEL INITIAL BOUNDARY VALUE PROBLEM.



SOURCE: AUTHOR.

The mechanical models used in the microstructure model's analysis can be represented by differential equations that relate stress and strains. In order to obtain the stress-strain relations of each model, three types of equations are used: i) kinetics (conservation of linear momentum), ii) kinematics (movement description) and iii) constitutive equations. Thus, the equations described below are sufficient to model the object:

- i. Kinetics (conservation of linear momentum):

$$\sigma_{ij} = 0 \text{ in } V \quad (1)$$

ii. Kinematics (movement description):

Considering small strains, the stress-strain relationship can be described by:

$$\varepsilon_{ij} = \frac{1}{2}(u_{ij} + u_{ji}) \text{ in } V \quad (2)$$

iii. Constitutive equations:

The constitutive equation for non-aging linear viscoelastic materials, including non-aged asphalt mixtures, are described as follows, respectively:

$$\sigma_{ij}(x_m, t) = \int_0^t E_{ij}(t - \tau) \frac{\partial \varepsilon_{ij}(x_m, t)}{\partial \tau} d\tau \quad (3)$$

Where,

E_{ij} : time-dependent linear-viscoelastic relaxation modulus tensor; t : time of interest; τ : time-history integration variable.

The initial condition for all state variables are known and assumed to be zero:

$$\sigma_{ij}(x_m, 0) = 0 \quad (4)$$

$$\varepsilon_{ij}(x_m, 0) = 0 \quad (5)$$

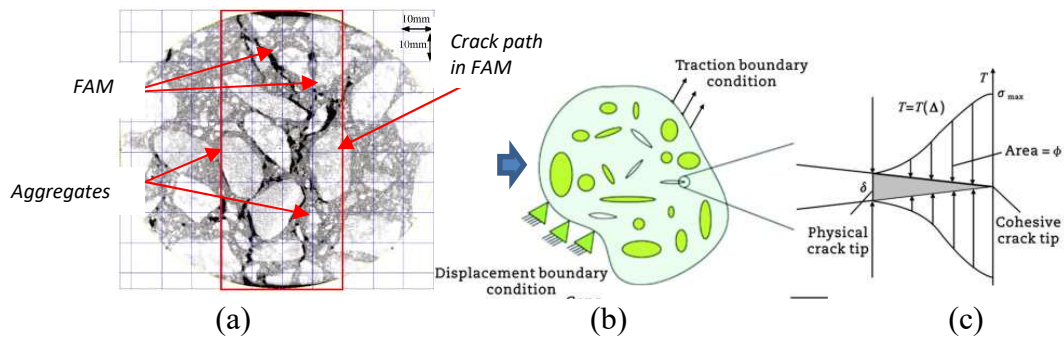
$$u_i(x_m, 0) = 0 \quad (6)$$

In the micromechanical approach, the phenomena of crack initiation and propagation is treated by means of discrete fracture models such as cohesive zone models (CZM). Through CZ models, the entire cracking phenomenon (crack initiation, propagation, nucleation and failure) can be modelled and observed and not only when the material collapses.

2.3. COHESIVE ZONE MODELS (CZM)

The first authors to introduced CZM were Dugdale (1960) and Barenblatt (1962). The CZM, as illustrated in Figure 6, represents the fracture as a gradual phenomenon that occurs in a potential damage zone ahead of a crack tip where fracture is resisted by cohesive tractions (T_n), that varies from a T_{max} to 0 (zero), when the fracture separation (δ_n) reached the critical cohesive displacement (δ_c) and full separations occurs.

FIGURE 6 - SCHEMATIC ILLUSTRATION OF COHESIVE ZONE MODELING CONCEPT.

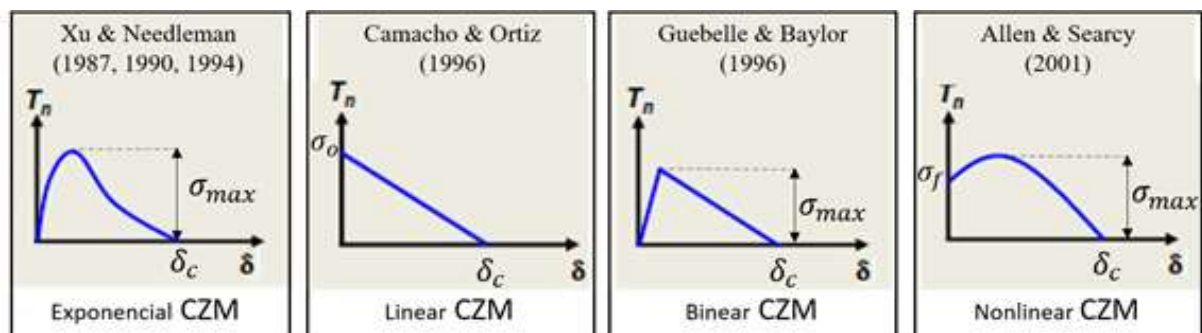


SOURCE: A) ADAPTED FROM HASSAN ET AL., 2014, AND B AND C) ADAPTED FROM KIM (2011).

Several researchers have been using CZM to perform fracture analysis in different kind of materials (ceramic, metals, polymers), including to investigate the fracture of asphalt concrete (SCHAPERLY, 1975; NEEDLEMAN, 1987; TVERGAARD, 1990; COSTANZO and ALLEN, 1993; ALLEN and SEARCY, 2001). For instance, Chang and Kaijian (2013) has used CZM to find the principles in low temperature fracture. During the study, the authors emphasize the advantages of CZM compared to traditional models of fracture analysis: (1) the non-linear property around the crack tip zone can be considered; (2) fracture path needs not be set in advance, and the fracture mechanism can be investigated; (3) the fracture zone length under different loads can be attained, and the crack propagation behavior can be well analyzed.

In summary CZM is an expression of fracture process zone that mechanically relates cohesive traction forces with separation displacement. Those constitutive relations, $T(\delta)$, are defined as softening curves. Several softening functions types have been proposed in the literature such as exponential (XU and NEEDLEMAN, 1987, 1990, 1994), linear (CAMACHO and ORTIZ, 1996), bilinear (GEUBELLE and BAYLOR, 1998), and non-linear (YOON and ALLEN, 1999; ALLEN and SEARCY, 2001). Figure 7 illustrates some CZM softening curves where they can be distinguished by two main characteristics: (1) the shape of the traction-separation curve and (2) the existence of an initial cohesive stiffness. Models with an artificial initial stiffness are called intrinsic models, while models that assume an initial rigidity are called extrinsic models.

FIGURE 7- EXAMPLES OF SOFTENING FUNCTIONS OF CZM PROPOSED IN THE LITERATURE.

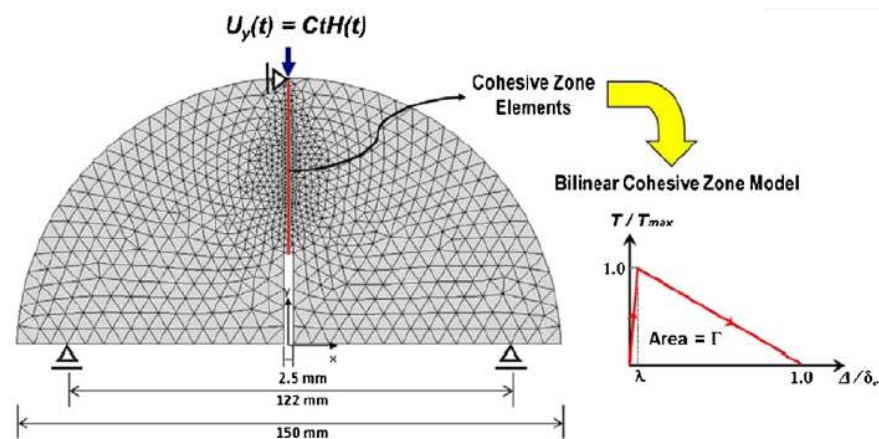


SOURCE: AUTHOR.

Several researches have been using CZM to evaluate fracture behavior in FAM. Aragão and Kim (2012) present an integrated approach combining experimental tests and numerical modeling to characterize mode I fracture behavior of FAM at intermediate temperature conditions using bilinear cohesive zone model (Figure 8). The model implemented by the author presented good agreement with experimental fracture test results. Cohesive strength and fracture energy parameters were determined at a wide range of loading rates and the study demonstrated that both fracture parameters are typically rate-related mainly at higher loading rates with insignificant rate-dependency at lower loading. Another

author's findings was about the fracture characteristics found by global measures. As the process of fracture is truly local phenomenon, the fracture energy parameters resulting from the global measurements shown to be overestimated which can mislead structural thickness design of pavement structures. The study shows that the energy dissipated by viscoelasticity play important role in the energy balance and for that it should be carefully considered when modeling fracture in viscoelastic media. In summary, the study demonstrated the importance of fracture models to well understand the rate-dependent behavior at the fracture process zone in the mixtures and the potential use of bilinear cohesive zone model to predicted fracture behavior of asphalt matrix by improving the methodologies to find the fracture parameters.

FIGURE 8 - A FINITE ELEMENT MESH AND ITS BOUNDARY CONDITIONS TO MODEL THE SCB TESTING

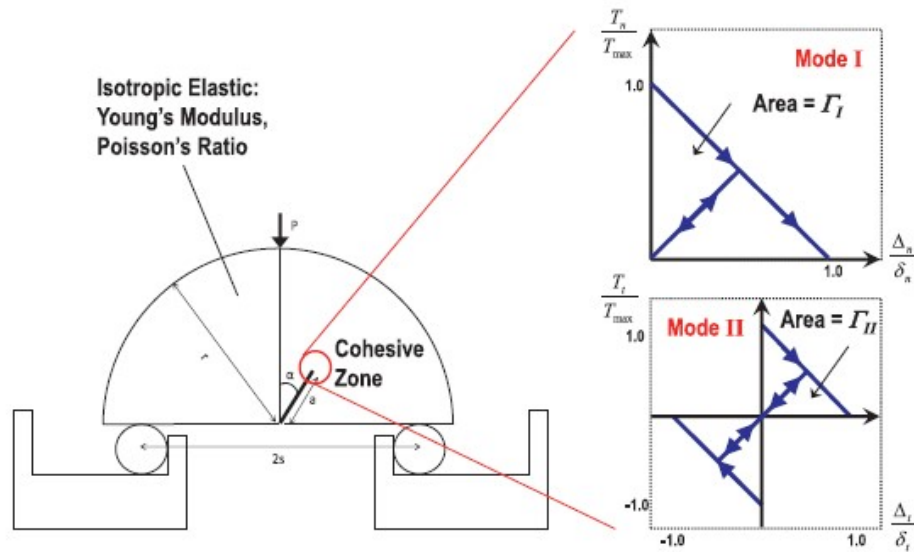


SOURCE: ARAGÃO AND KIM (2012).

Im et al. (2014) and Ban et al. (2015) incorporated into finite element model simulations the linearly decaying mixed-mode cohesive zone model to characterize mode-I and mode-II fracture properties of FAM (Figure 9). The authors intended to find a comprehensive understanding to the mode-dependent fracture characteristics of asphalt mixtures using only FAM mixture. The author's findings clearly indicate that the fracture characteristics need to be well understood when pursuing a more accurate design of pavement structures. An important conclusion from the studies is that the mode-II fracture toughness is

about three times greater than mode-I fracture toughness, which implies that FAM mixtures are approximately more resistant to the sliding mode than the opening failure, thus the mode-dependent fracture characteristics should be considered in the design process of pavement structures for a more accurate prediction of the crack-related distress such as fatigue cracking and thermal cracking.

FIGURE 9 - ILLUSTRATION OF THE SCB SPECIMEN WITH ITS MATERIAL PROPERTIES THE LINEARLY DECAYING MIXED-MODE COHESIVE ZONE MODEL.



SOURCE: IM ET AL. (2014).

Many previous studies have applied CZM for predicting fracture of asphalt mixtures via intrinsic bilinear CZM. Bilinear CZM assumes that there is a recoverable linear elastic behavior until the traction (T) reaches a peak value, or cohesive strength (T_{max}) at a corresponding separation in the traction–separation curve. At that point, a non-dimensional displacement (λ_{cr}) can be identified and used to adjust the initial slope in the recoverable linear elastic part of the cohesive law (KIM and ARAGAO, 2013). Several researchers have reported numerical issues associated with artificial compliance in the response of the bodies of interest to externally applied loads due to the assumption of the initial artificial stiffness in the traction-separation relations of intrinsic models (GEUBELLE and BAYLOR 1998, ESPINOSA et al. 2000, ALFANO and CRISFIELD 2001, KLEIN et al. 2001, ZAVATTIERI and ESPINOSA 2001, ESPINOSA and ZAVATTIERI 2003, SONG et al. 2006). Moreover,

it is required the insertion of CZ elements a priori within the finite element mesh and it may become computationally expensive. In contrast, extrinsic CZM is probably more realistic than the intrinsic approach, because they do not assume the pre-existence of CZ elements within the finite element meshes. Cohesive elements are inserted as needed by node duplication (the process generally referred to as dynamic or adaptive insertion) in the mesh whenever a damage initiation criterion is reached. There are a few studies that consider extrinsic CZM and viscoelasticity in the fracture process of asphalt media (KIM, 2003; SOUZA et al., 2004; TEIXEIRA et al., 2014). It is well known that asphalt mixtures are time and rate-dependent viscoelastic and it is believed herein that cracking phenomena can thus be better described and predicted using nonlinear viscoelastic cohesive zone (NVCZ).

Thus, this study used the extrinsic NVCZ model proposed by Allen and Searcy (2001) to predict fracture behavior of asphalt composites. The NVCZ model used herein and effects of each NVCZ parameters on asphalt material's cracking evolution is the aim of this research. This can lead to a better understanding of the fracture behavior of different types of HMA mixtures. In this model, cohesive zone elements are inserted in the body if the stress in the material reaches certain level, denoted by σ_f , which is defined as the requisite stress level to initiate cohesive zones. As the material continues to be loaded, cohesive tractions increase until reaches σ_{max} . After that point, cohesive tractions start to decrease until reaches zero. At this stage, the critical cohesive displacement (δ_c) is reached and material separation occurs. The model used in this study is described by the following non-linear rate dependent traction-separation relationship:

$$T_{i(t)} = \frac{1}{\lambda(t)} \frac{\delta_i(t)}{\delta_i^*} [1 - \alpha(t)] \cdot \left[\sigma_i^f + \int_0^t E^c(t - \tau) \frac{\partial \lambda(\tau)}{\partial \tau} d\tau \right] \quad (7)$$

where,

$T_i(t)$: traction forces acting on the cohesive zone boundary;

$\delta_i(t)$: cohesive zone opening displacement;

δ_i^* : material length parameter i direction;

$\alpha(t)$: internal damage parameter;

σ_i^f : required stress level to initiate damage;

$E_c(t)$: time-dependent relaxation modulus of cohesive zone;

$\lambda(t)$: Euclidean norm of the damaged zone opening displacements, given by:

$$\lambda(t) = \left[\left(\frac{\delta_n(t)}{\delta_n^*} \right)^2 + \left(\frac{\delta_r(t)}{\delta_r^*} \right)^2 + \left(\frac{\delta_s(t)}{\delta_s^*} \right)^2 \right]^{\frac{1}{2}} \quad (8)$$

Where δ_n , δ_r and δ_s are the n; r; s- components of the damage zone opening displacements, and δ_n^* , δ_r^* and δ_s^* are empirical material length parameters.

In order to complete the model description, it is necessary to construct an internal variable evolution law for the internal damage parameter $\alpha(t)$ which is responsible for characterizing the state of damage. It can be notice from Equation (7) that when $\alpha(t)$ reaches 1 the traction force, $T_i(t)$, goes to 0, meaning that the faces of the cohesive element are fully separated. The damage evolution law that has been chosen for this study is the same as the one in Allen and Searcy (2001), which is a simple rate dependent generalization of the continuum damage formulation proposed by Kachanov (1958) and Rabotnov (1969), given by:

$$\dot{\alpha} = A\dot{\Lambda}^m \quad \dot{\Lambda} \geq 0 \text{ and } \alpha \geq 0 \quad (9)$$

$$\dot{\alpha} = 0 \quad \dot{\Lambda} \leq 0 \text{ or } \alpha = 0 \quad (10)$$

Where A and m are the material damage parameters. NLVE- CZM formulation shown above has been applied in many studies to preview damage evolution in many materials, as inelastic polycrystalline solids (HELMS et al.,1999) and composite materials (PHILLIPS et al., 1999; SEIDEL et al., 2005). Its use for modelling asphaltic media is still incipient, with few studies published for pavement mechanics application (KIM, 2003; SOUZA et al., 2004; LUTIF et al., 2012).

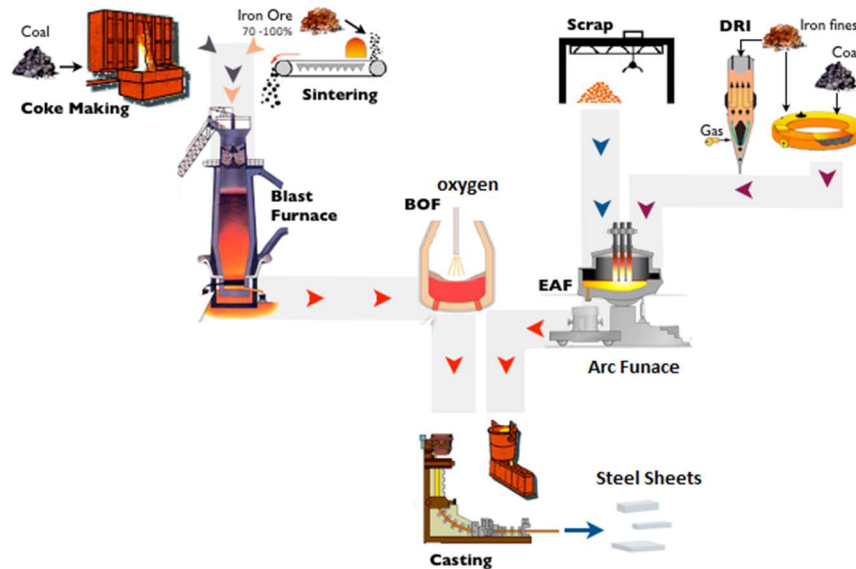
Aragão (2011) correlates some of the main factors that still limit the predictive capabilities of computational models, such as: the heterogeneity and the inelastic constitutive responses of the mixtures; the relatively large deformations in the fracture process zone of the mixtures; the rate-dependent characteristics of that fracture process zone; the difficulties associated with the proper characterization of rate-dependent fracture properties and with the development of fracture models that consider the rate-dependence of those properties, among others.

2.4 USE OF LD STEEL SLAG AS FILLER IN ASPHALTIC MATERIALS

An important industrial sector in the world, responsible for a significant amount of residue's production, is the steel making industry. According to the World Steel Association (WSA), in 2016, world crude steel production reached over 1.63 billion metric tons. Brazillian production occupies the ninth position, with a 31.3 million tons crude steel production, according to Brazilian steel institute (IAB, 2016). The state of Espirito Santo (ES) was responsible for 24% of the total amount of steel produced in Brazil, that is 7.5 million tons.

Each integrated steel plants have their process of production that can be laid out in various combinations depending on product mix, available raw materials, energy supply and investment capital. Therefore, there are three main process of crude steel production: In Blast Furnace (BF)/Basic Oxygen Furnace (BOF) route, Scrap/Electric Arc Furnace (EAF) route and Direct Reduced Iron (DRI)/EAF route. The three routes are schematic summarized in Figure 10.

FIGURE 10 - SCHEMATIC ILLUSTRATION OF STEEL PRODUCTION BY THREE DIFFERENT ROUTES.



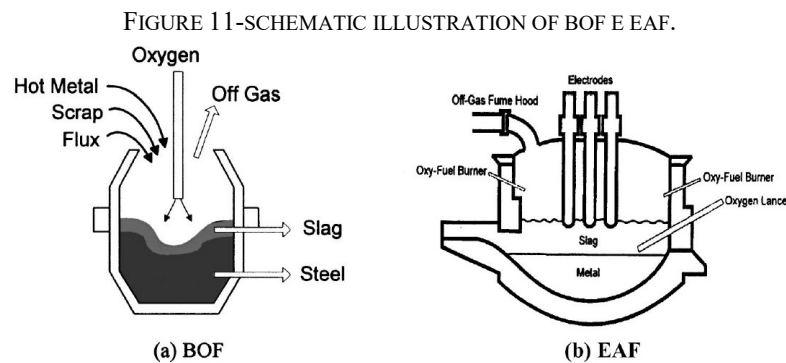
SOURCE: ADAPTED FROM INSTITUTE FOR INDUSTRIAL PRODUCTIVITY.

Steel Slag is a byproduct of steel production from either the melting of scrap to make steel in electric arc furnaces (EAF), or conversion of iron to steel in basic oxygen furnace (BOF). In the manufacturing processes the furnaces are charged with the predetermined mixture of raw material, i.e., scrap, pig iron, fluxes – lime (CaO and dolomitic lime). The amount of each material varies from 60% steel scrap with 40% pig iron to 90% steel scrap with 10% pig iron, this variation depends on material prices and local availability.

In the process called LD (Linz-Donawitz) or BOF (Basic Oxygen Furnace), Figure 11 (a), the steel is produced by reducing hot liquid metal by injecting hot natural oxygen. The oxygen combines with controlling the carbon percentage and removing the material

impurities. The flux agents combine with these impurities during the process to form the steel slag. At the end of the refining operation, the liquid steel is separated from the slag by decantation process (SHI, 2004; GERDAU S.A., 2001).

In EAF process, cold steel scraps are used, reducing the amounts of iron scrap, pig iron, and direct reduced iron. After charging the electric arc furnace with the predetermined mixture of raw materials, electric power is applied following a computer-controlled melting profile, Figure 11 (b), (SHI, 2004; GERDAU S.A., 2001).



SOURCE: SHI (2004).

The steel slag chemical compounds presented in the steel slag from those two furnaces are very similar. They consist primarily of CaO, MgO and FeO. Moreover, the proportion of these oxides and other components changes according to steel refine process (BOF, EAF, or others), raw materials used (type of coal, coke, and iron ore) and furnace conditions. Table 1 shows the chemical composition of steel slag from different plants of steel production from BOF process.

TABLE 1 - CHEMICAL COMPOSITION OF BOF SLAG FROM MANY RESEARCHERS.

Compounds	Mahieux et. al (2009)	Belhadj et. al (2012)	Diao et. al (2016)	Cosme et. al (2016)	Freitas et al. (2018)
CaO	47.5 %	45.0 %	35.31%	36.78%	45%
SiO₂	11.8 %	10.8%	13.7%	14.17%	8.4%
Fe₂O₃	22.6 %	32.0%	25.95%	24.36%	21.2%
Al₂O₃	2.0 %	1.9%	2.66%	7.55%	3.9%
MgO	6.3 %	4.5%	12.42%	11.54%	6.1%
MnO	1.9%	2.6%	3.81%	3.83%	-
P₂O₅	2.7%	1.4%	2.07%	0.94%	-
TiO₂	0.5%	0.5%	2.17%	0.38%	-

SO₃	0.2%	0.4%	-	0.14%	-
-----------------------	------	------	---	-------	---

SOURCE: AUTHOR.

The material is a complex matrix structure consisting primarily of simple oxides determined from elementary analysis of x-ray fluorescence. Steel Slag usually contain four major oxides CaO, MgO, SiO₃ and Fe₂O₃, namely lime, magnesia, sílica and hematite, respectively. Minor elements include sulfur, aluminium, manganese, alkalis and trace amount of several others. The Fe₂O₃ present in the steel slag contributes to a greater stiffening of the asphalt mixture, which can increase to the formation of cracks in the asphalt coating if it is subjected to low temperature conditions (Yoon and Tarrer, 1988), so the existence of it and other metals in slag material contributes greatly to the appreciable resistance of LD steel slag to abrasion. The high concentration of CaO increases the material's performance reducing wheel track rutting, as well as aging and stress-related cracking (Little, 2006). Lastly, the presence of SiO₂ can affect negatively the asphalt concrete performance, as silica prejudices the adhesiveness between binder aggregate (Yoon and Tarrer,1988).

As said before, the main concern about steel slag application as aggregates into asphalt mixtures consists in their volumetric instability. The CaO hydrates very quickly causing instantaneous volumetric variations in the grains. Also, the hydration of MgO compound is slow, which take years until material reaches the stabilization, and may cause volumetric changes over time. In this aspect the use of this by-product as a filler in asphalt pavements becomes highly attractive since the fineness of the material can minimize the problems of expansion of the material. The authors Gottardi (2015), Cosme et al. (2016) and Fonseca (2016) evaluated the incorporation of steel slag in the performance of asphalt binders under three approaches

Cosme et al. (2016) evaluated the influence of the addition of filler of steel slag LD on the rheological properties of the asphalt mastic and its susceptibility to permanent

deformations by means of frequency sweep tests, creep and multiple stress creep recovery (MSCR) tests. The authors compared mastics with incorporation of fillers of two by-products (steel slag and ornamental stones). The results showed that the use of steel slag increased the G^* of the mastic significantly compared to mastics produced with ornamental stone residues. According to the authors, the higher G^* values for mastics with LD slag may be linked to the higher concentration of iron oxide and lower impurity (silica) levels than the OSR residue; this factor may have contributed more to the hardening of the mastic than to the increased concentration of fine grains in the OSR residue. The creep and recovery analyses showed that the LD slag mastics are less likely to be permanently deformed than the ones that contain ornamental stone residues, probably due to the greater grain diameter of fillers for the slag.

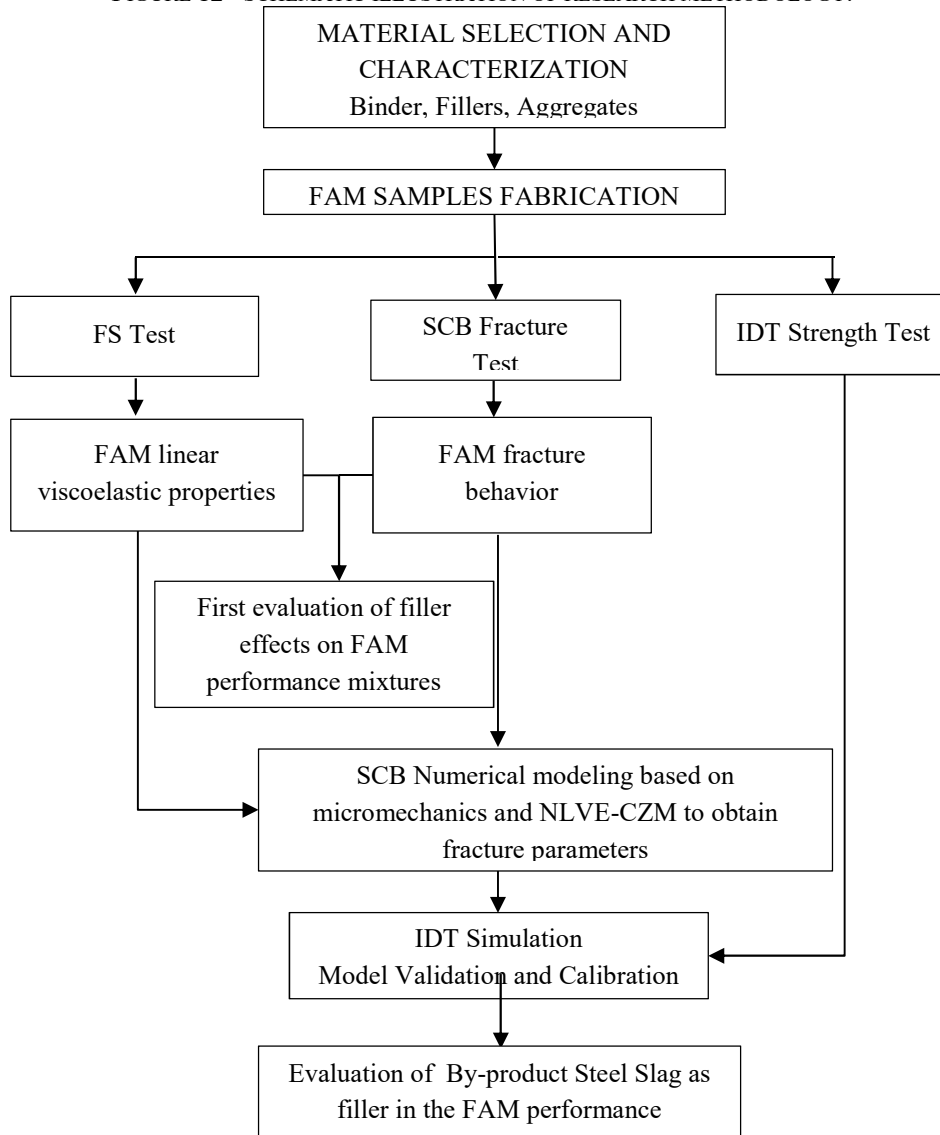
Fonseca (2016) evaluated the effect of LD steel slag on FAM characteristics and compared with FAM with hydrated lime addition results. Analysis of stiffening effect, fatigue resistance and fracture behavior were conducted on FAM specimens by means of frequency sweep tests, time sweep tests fitted in a viscoelastic continuum damage model (VECD) and Semi Circular (SCB) fracture tests. Regarding influence of fillers on material rigidity, for high frequencies mixtures with hydrated lime slag presented higher G^* than FAM with LD slag, and at low frequencies the results were not significantly different. From VECD analysis, FAM with hydrated lime showed lower material integrity for the same level of damage accumulation than FAM with LD slag. Also, based on fracture parameters from SCB test, FAM with hydrated lime presented lower fracture energy than FAM with LD steel slag.

Although these studies used advanced laboratory tests to characterize materials, the fracture and damage mechanisms of the mixtures that originate in the microstructure of the material under the influence of the interactions between the various constituents have not been well understood. Therefore, the use of microstructure modelling with NLVE-CZ model could be a power tool to assess fracture phenomena and to explain the abovementioned results.

3. EXPERIMENTAL PROGRAM

This chapter presents materials and methodology used in this the research. Testing procedures of the individual constituents and the FAM studied mixtures are presented.

FIGURE 12 - SCHEMATIC ILLUSTRATION OF RESEARCH METHODOLOGY.



SOURCE: AUTHOR.

Firstly, the materials used for FAM preparation and fabrication were properly selected and characterized. FAM samples were fabricated, and laboratory tests were performed to obtain the constitutive properties for the two FAM mixtures studied, differentiated by the filler addition on them, i.e., steel slag or and hydrated lime, named herein as FAM_HL and

FAM_SS, respectively. Frequency Sweep Tests (FS) were conducted to obtain viscoelastic properties of FAM mixtures and semi-circular bending tests (SCB) were performed to obtain fracture parameters of mixtures. The software MultimechTM was used to perform numerical simulations. To validate the model, indirect tensile strength tests (IDT) were conducted in laboratory and experimental results were compared with the numerical model results.

3.1 MATERIAL CHARACTERIZATION

3.1.1 Asphalt binder

An asphalt binder PG 70-28 was used. It was provided by a local asphalt mixture plant (*Usina Terra Brasil* co.). The binder characteristics were provided by the supplier refinery REGAP/PETROBRAS and are shown in Table 2. They are in accordance with the Brazilian specifications regulated by the Petroleum National Agency (ANP, 2005).

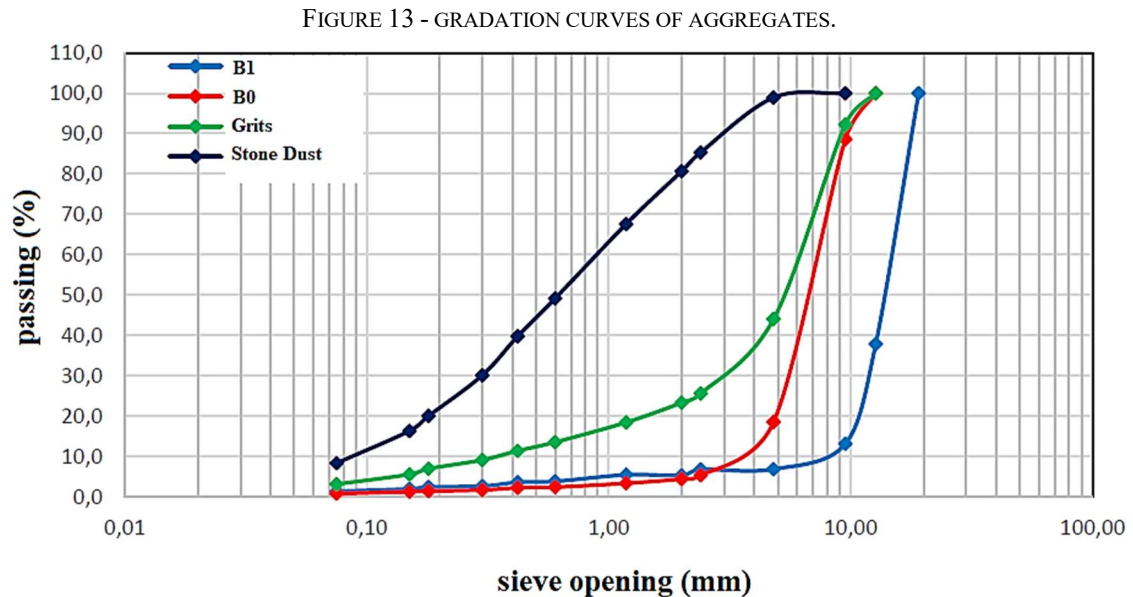
TABLE 2 - ASPHALT BINDER CHARACTERIZATION.

Característica	Method	Specification	Results	Unit
Penetration	ASTM D5	50 to 70	53	0,1 mm
Softening Point	ASTM D36	46 min	49.4	°C
Brookfield Viscosity 135GC SP21 20RPM	ASTM D 4402	274 min	300	cP
Brookfield Viscosity 150GC SP21	ASTM D 4402	112 min	153	cP
Brookfield Viscosity 177GC SP21	ASTM D 4402	57 a 285	58	cP
RTFOT Retained Penetration	ASTM D5	55 min	62	%
RTFOT Increased Softening Point	ASTM D36	8max	4,2	°C
RTFOT Ductility 25GC	ASTM D113	20 min	>150	cm
RTFOT % mass variation	ASTM D2872	(-)0,50 a 0,50	-0.226	%
Ductility 25GC	ASTM D 113	60 min	>150	cm
Solubility in Trichloroethylene	ASTM D 2042	99,5 min	99.9	% mass
Flash Point	ASTM D92	235 min	338	°C
Heat susceptibility index	ASTM X 018	(-)1,5 a 0,7	-1.2	N/A
Specific Gravity - 20/4 GC	ASTM D70	-	1.008	N/A

SOURCE: REGAP LABORATORY.

3.1.2 Aggregates

Three types of granite aggregates were used (B1, B0, Grits and Stone). Figure 13 and table 3 shows the aggregate's particle-size distribution (PSD) and physical characteristics, respectively.



SOURCE: ADAPTED FROM GOTTARDI (2015).

TABLE 3 - PHYSICAL CHARACTERISTICS OF THE AGGREGATES.

Aggregate	Real Specific Mass (g/cm ³)	Los Angeles Abrasion	Sand Equivalent
B1	2.793		
B0	2.791	55.87%	-
Grits	2.817		
Stone Dust	2.79		67.5%

SOURCE: GOTTARDI (2015).

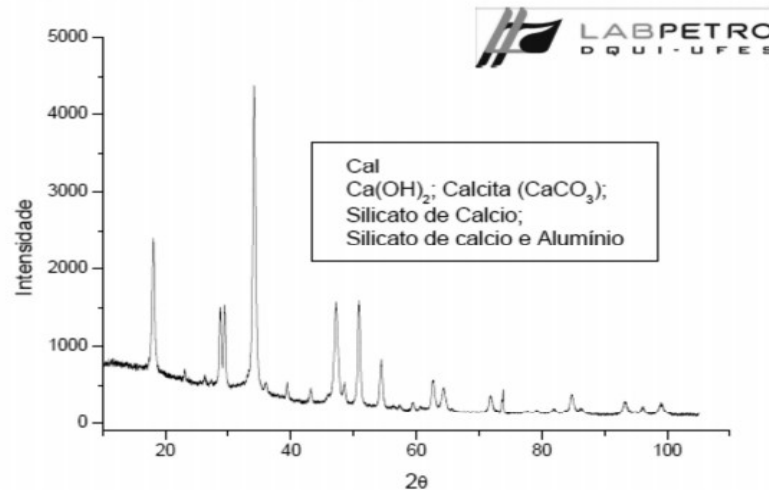
3.1.3 Fillers

a) Hydrated Lime

The hydrated lime used was a commercially available from *Massical co*. The material was oven dried at 105 ° C and stored inside plastic bags prior its use. Its specific mass value obtained was 2.205 g/cm³. Mineralogical analysis by X-ray diffraction was also carried out

and the diffractometer results are shown in Figure 14. As expected, it is possible to notice the presence of calcite, followed by calcium and aluminum silicates.

FIGURE 14 - MINERALOGICAL CHARACTERISTICS OF HYDRATED LIME PARTICLES.



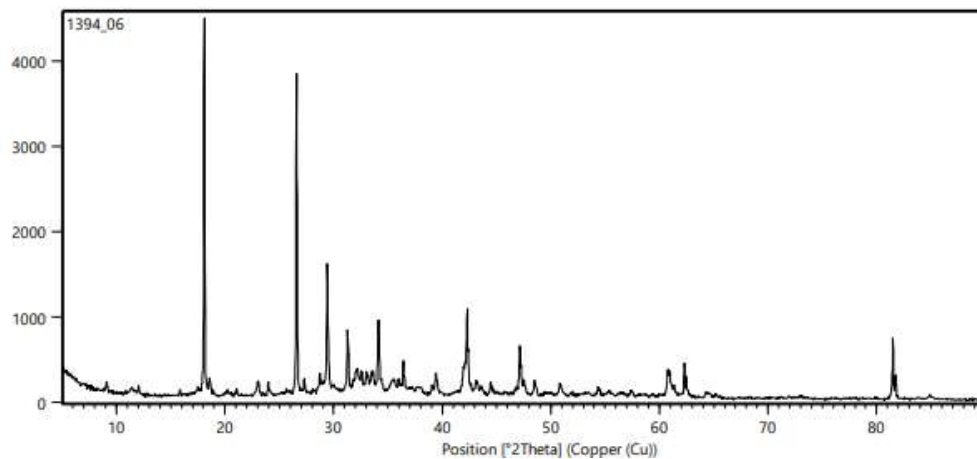
SOURCE: LABPETRO REPORT

b) LD steel slag

For the present study, LD steel slag with expansion level reduced to 3%, commercially named as ACERITA, provided by *Arcelor Mittal Tubarão co.* located in Serra (ES-Brazil), was selected. The LD slag was the same used in other studies (Gottardi, 2015, Cosme et. al. 2016, and Fonseca, 2016). The material was first oven dried at 105 °C, then passed in the sieve #200 (0.075 mm), homogenized, quartered and stored inside plastic bags.

Specific mass value obtained was 2.91 g/cm³. Mineralogical analysis by X-ray diffraction was also carried out and the result is shown in Figure 15. From the analyses it is possible to notice the presence of Magnetite (Fe₂O₄), Quartz (SiO₂), Calcite (Ca₂CO₃) and others.

FIGURE 15-MINERALOGICAL CHARACTERISTICS OF LD STEEL SLAG PARTICLES.



SOURCE: NANOBUSINESS INOVAÇÃO E INFORMAÇÃO REPORT.

Chemical characterization of the by-product was also performed by X-ray fluorescence spectrometry (FRX) and the results are shown in Table 4. From the results, it can observe a large amount of calcium oxide (CaO), iron oxide (Fe₂O₃) and silicon oxide (SiO₂). According to Cosme et al. (2016), the iron oxide present in the slag contributes to a greater stiffening of the asphalt mixture.

TABLE 4 - SEMI-QUANTITATIVE ANALYSIS IN THE FORM OF OXIDES OF THE STEEL SLAG BY FRX.

Oxides	(%)
Na ₂ O	0,17
MgO	5
Al ₂ O ₃	4,9
SiO ₂	12,7
P ₂ O ₅	1,3
SO ₃	0,16
K ₂ O	<0,1
CaO	43,4
TiO ₂	0,36
MnO	3,2
Fe ₂ O ₃	26,4
SrO	0,1
LC*	1,6

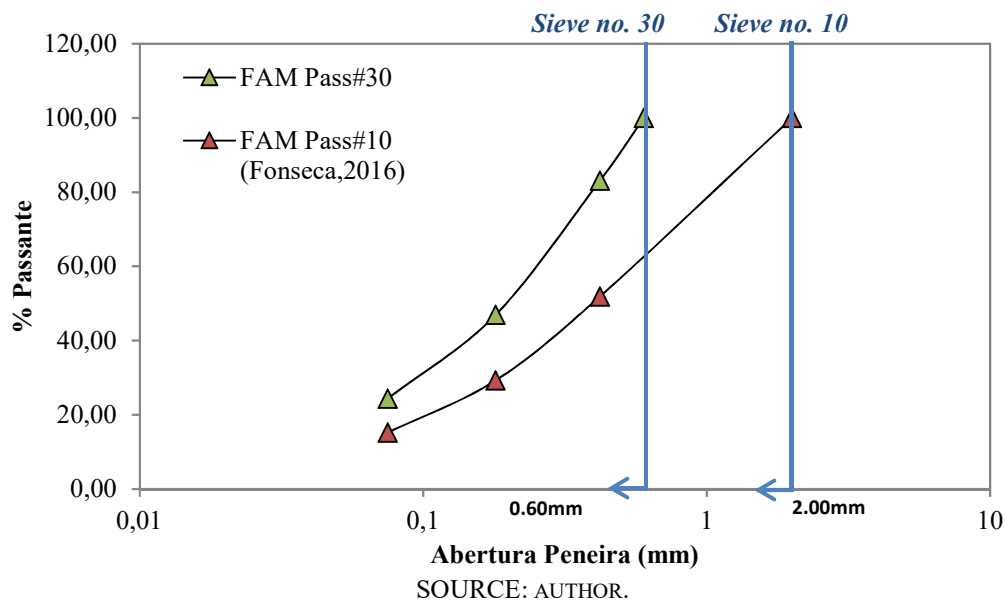
*LC = Loss by Calcination

SOURCE: NANOBUSINESS INOVAÇÃO E INFORMAÇÃO REPORT.

3.2 FAM MIX DESIGN

The main purpose of this study was to evaluate the effect of LD steel slag in replacement of hydrated lime on FAM characteristics, as well as to investigate the efficiency-validity of the extrinsic NVCZ model for characterizing case-specific fracture properties and predicting fracture behavior of asphaltic materials. FAM was selected based on Fonseca (2016) FAM gradation. However, Fonseca (2016) considered particles smaller than 2.00mm while herein only particles smaller than 0.60 mm (No. 30 sieve) were used. Binder content of 13.3% by total weight of FAM mixture were produced and tested. It is important to mention that there is no consensus on the literature about the nominal maximum aggregate size to represent FAM phase. Figure 16 shows the gradation curves of HMA from Gottardi (2015) and the respective derived PSD for the FAMs used in this study.

FIGURE 16- GRADATION CURVES OF THE FINE AGGREGATE MATRIX AND THE COMPLETE BITUMINOUS COMPOSITE.



The percentage of 7.43% (by total FAM mass) of hydrated lime and LD steel slag were added in FAM_HL and FAM_SS, respectively. The binder content was kept the same to eliminate binder content influence on the results and equal to 13.3% for both mixtures studied herein, since the main objective was to evaluate exclusively the influence of the filler in asphalt matrix performance.

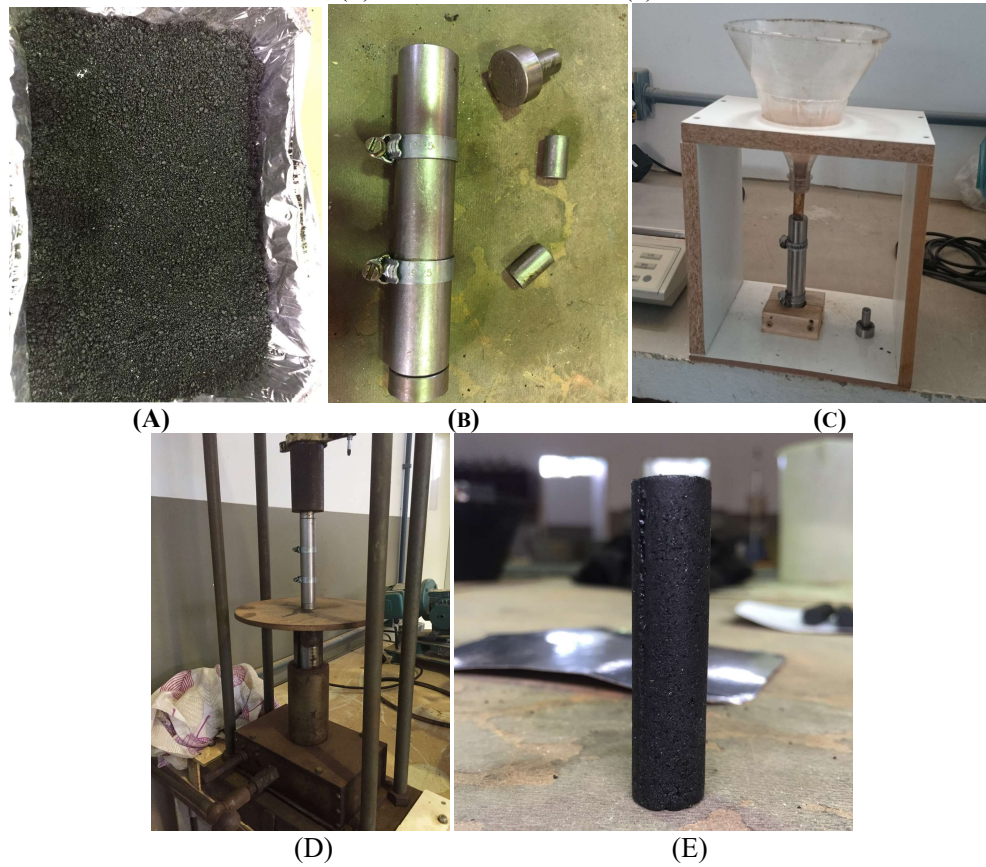
3.3 LINEAR VISCOELASTIC PROPERTIES OF FAM_SS AND FAM_HL

Linear viscoelastic properties of the studied FAM were experimentally obtained by performing dynamic frequency sweep (FS) tests using a dynamic shear rheometer (DSR) followed by the curve fitting collocation method to obtain Prony Series coefficients.

3.3.1. DSR sample fabrication

For each FAM (FAM_HL and FAM_SS) four cylindrical samples with 50 mm diameter and 12mm height were fabricated. The procedure to fabricate (mixing and compaction) these testing samples was based on Fonseca (2016) and included some step, as follow: first, aggregates were quarter, dried and sieved. For each studied FAM, 500g of mixture was prepared by preheating the aggregates and the binder to the mixing temperature of 146 °C for 2 hours and then mixed at 135 °C. After that, the mixture was put inside a container, as shown in Figure 17 (a), and small amounts were heated for short time at 135°C as needed to compaction. The amount of mixture necessary to mold each sample was experimentally determined by attempts targeting samples with 4.00 +/- 0.5% of air voids. Figure 17 (b) and (c) show the bipartite mold used and the apparatus to place sample inside the mold, respectively. To compact the samples, it was used a mechanical pressing machine, with a manual compactation effort, as displayed in Figure 17 (d). After compaction, the sample was removed by opening the brackets and separating mold parts. Figure 17 (e) shows one example of FAM sample used for DSR testing. Table 5 summarizes the volumetric parameters obtained of FAM samples for DSR testing.

FIGURE 17 - FAM SAMPLE FABRICATION PROCESS: (A) FAM MIXTURE BATCH; (B) SAMPLE MOLD; (C) MIXTURE BEING PLACED IN THE MOLD; (D) SAMPLE COMPACTION; (E) FAM DSR TESTING SAMPLE.



SOURCE: AUTHOR.

TABLE 5 - VOLUMETRIC PARAMETERS OF TESTING SAMPLES.

FAM	Mixture Mass (g)	Dried Mixture Mass (g)	Submerged Mass (g)	Gmb	Air Voids (%)
FAM_HL	13.3	13.21	7.18	2.191	3.89
		13.19	7.16	2.187	4.04
		13.23	7.17	2.183	4.22
		13.22	7.21	2.199	3.50
FAM_SS	15.5	14.94	8.25	2.233	3.64
		14.94	8.22	2.223	4.07
		14.77	8.14	2.227	3.87
		14.79	8.17	2.234	3.60

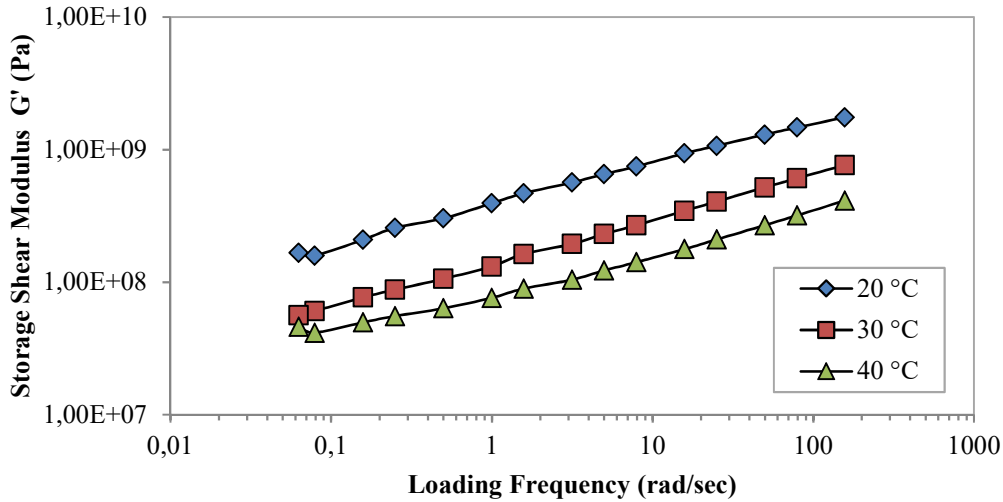
SOURCE: AUTHOR.

3.3.2 FAM Linear Viscoelastic Properties

The studied FAMs were subject to dynamic frequency sweep tests by applying a controlled strain amplitude of 65 microstrains and varying the frequency from 25 Hz to 0.01 Hz at three different temperatures (20°C, 30°C and 40°C).

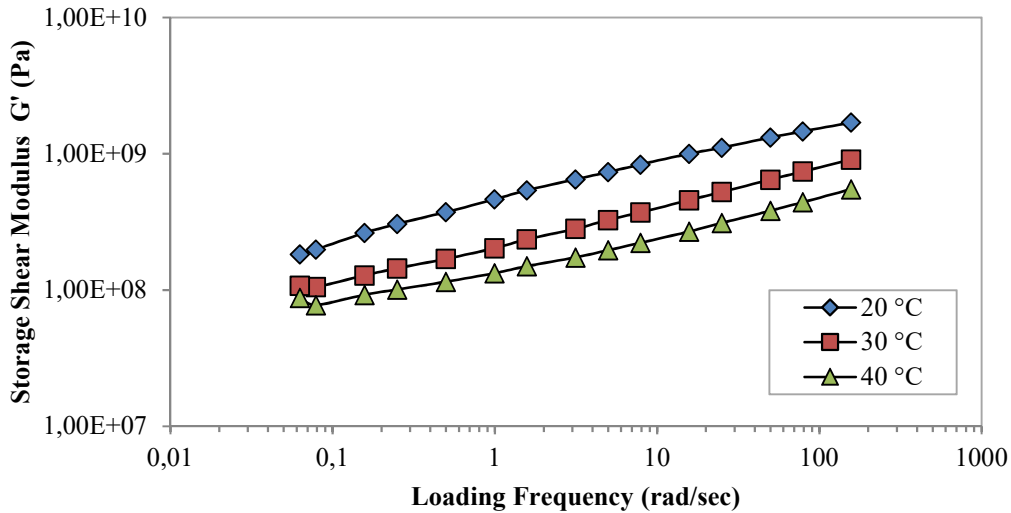
Storage Shear Modulus over the reduced frequency domain were plotted at the three temperatures. Figure 18 and Figure 19 shows the results for FAM_HL and FAM_SS, respectively. Four samples were tested for each mixture and the averaged values were used for collocation method.

FIGURE 18 - FREQUENCY SWEEP TEST RESULTS - FAM_HL.



SOURCE: AUTHOR.

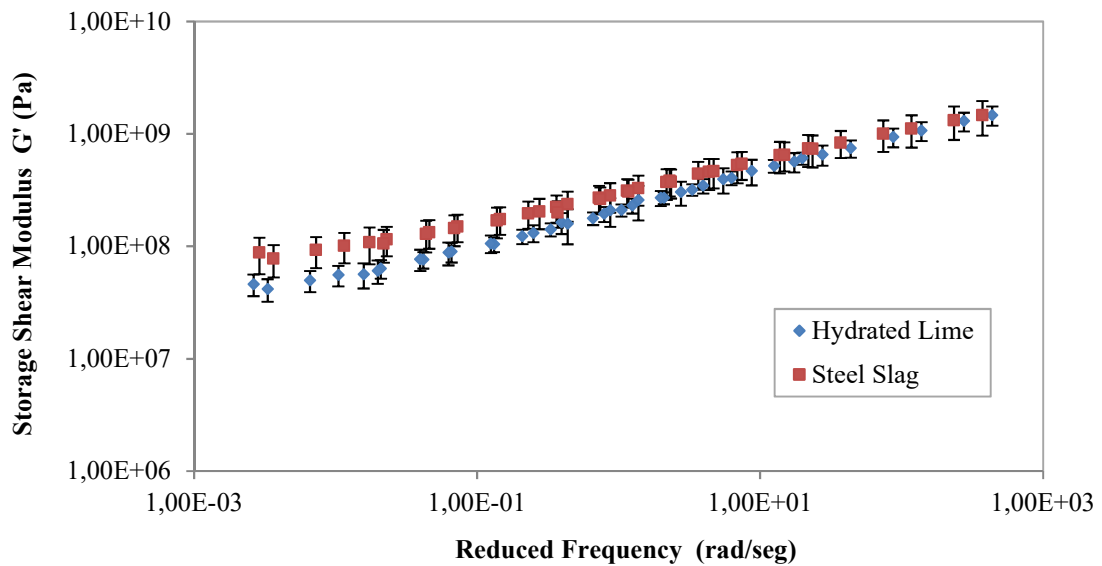
FIGURE 19 - FREQUENCY SWEEP TEST RESULTS - FAM_SS



SOURCE: AUTHOR.

With results shown above and employing temperature superposition principle, the linear viscoelastic master curves of the storage modulus in the frequency domain at a reference temperature of 25 °C were obtained for the FAM_HL and FAM_SS, as shown in Figure 20.

FIGURE 20- MASTER CURVE OF DYNAMIC SHEAR MODULUS FOR THE ASPHALT MATRIX AT 25 °C.



SOURCE: AUTHOR.

In concern about the filler effect in the mixture viscoelastic stiffness characteristics, from Figure 20 is possible to observe that at high frequencies the dynamic shear moduli were similar to both mixtures, FAM_SS and FAM_HL, but at low frequencies is noticed higher values for FAM_SS, which means that the steel slag filler increased the material stiffness mainly at high temperatures (low frequencies) improving the material resistance of permanent deformations. According to Bahia (1995) the effects of the filler incorporation on asphalt matrix are more significant and favorable at high temperatures (low frequencies), increasing the stiffness of the binder, which has a smaller complex modulus in this temperature range. However, at low temperatures, the filler further increases the stiffness of the asphalt binder, resulting in a reduction in the capacity to relax tensions, which means that in this aspect the incorporation of the by-product steel slag improved the performance of the asphalt mixture. This increased stiffness observed in the FAM_SS can be explained by the higher specific mass of the slag compared to the specific mass of lime, 32% higher. Besides that, as already mentioned above the presence of iron oxide (Fe_2O_3) in relatively high concentrations contributes to a greater stiffening of the asphalt mixture (COSME et. al. 2016).

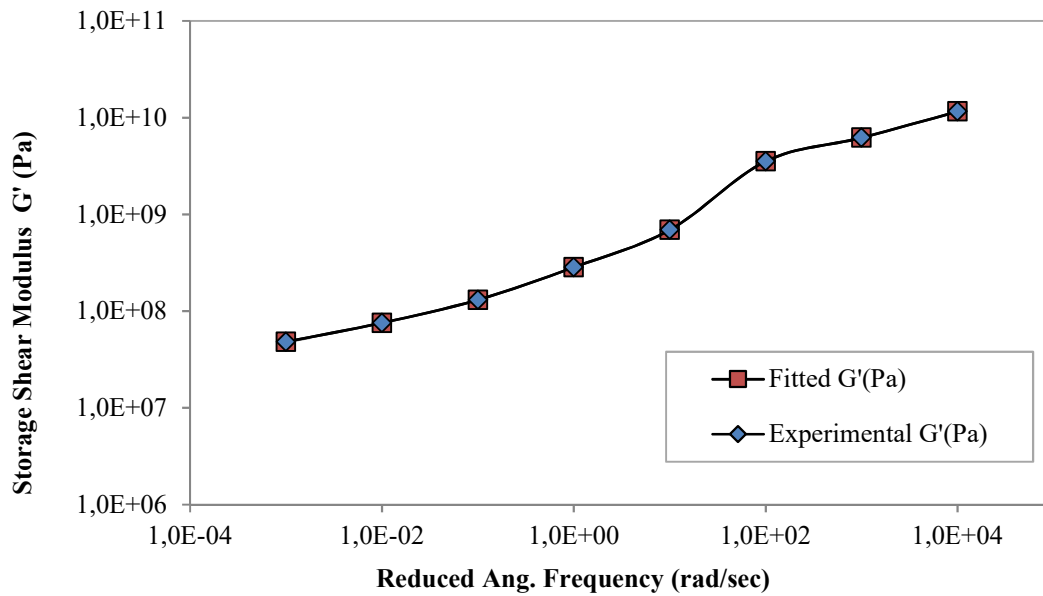
Following the procedure described in (KIM, 2003) and already applied by other researchers (SOUZA, 2005; LUTIF, 2011; ARAGÃO, 2011), the Prony series coefficients were used to define time-domain shear relaxation modulus. Poisson's ratio of 0.30 was assumed base in (BERNUCCI, 2006). TABLE 6 shows the linear viscoelastic properties for the FAM's used herein (spring constants (E_i) and relaxation time (ρ_i) in the generalized Maxwell model).

TABLE 6 - PRONY SERIES COEFFICIENTS OF THE MATRIX PHASE AT 25°C.

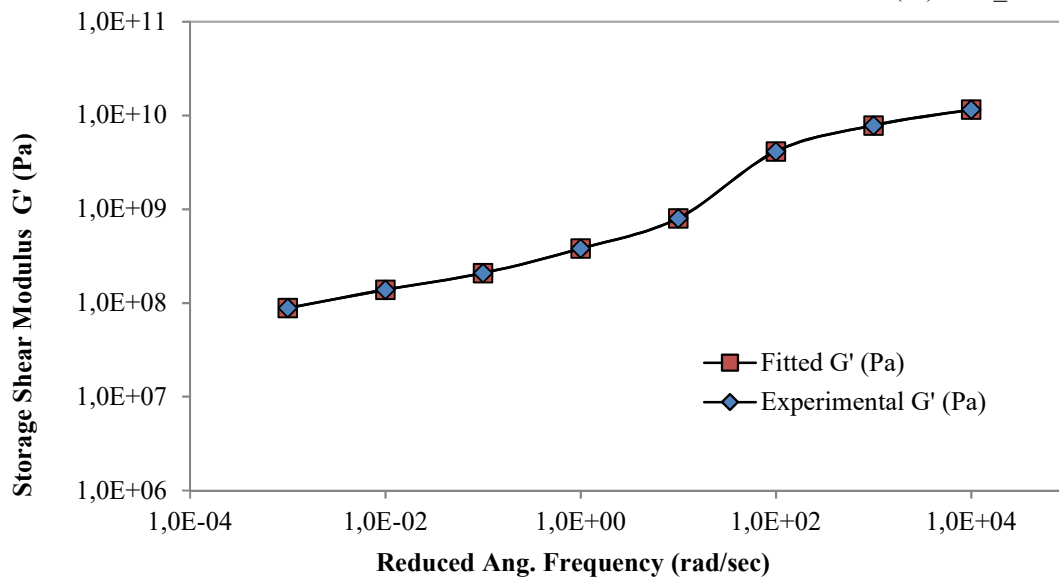
FAM mixtures		FAM_HL		FAM_SS
ρ_1	1.10E-04	E_1	9.39 E+09 Pa	5.23E+09 Pa
ρ_2	1.10E-03	E_2	7.04 E+08 Pa	1.95E+09 Pa
ρ_3	1.10E-02	E_3	4.91 E+09 Pa	5.83E+09 Pa
ρ_4	1.10E-01	E_4	4.68 E+08 Pa	4.41E+08 Pa
ρ_5	1.10E+00	E_5	2.19 E+08 Pa	2.60E+08 Pa
ρ_6	1.10E+01	E_6	6.56 E+07 Pa	6.01E+07 Pa
ρ_7	1.10E+02	E_7	3.93 E+07 Pa	7.70E+07 Pa
ρ_8	1.10E+03	E_8	1.24 E+07 Pa	1.89E+07 Pa
		E_∞	4.10 E+07 Pa	7.70 E+07 Pa

SOURCE: AUTHOR.

The results generated for the storage modulus (G') over the frequency domain using the Prony Series coefficients were compared with experimental results, to verify the propositions of linearity and negligible inertia assumed in the development of the mechanical models, represented by Prony series. Figure 21 and Figure 22 present the results for FAM_HL and FAM_SS, respectively. It is observed that there were no significant variations in the curves, which indicates that the fitting procedure used was valid.

FIGURE 21 - CURVES OF EXPERIMENTAL AND FITTED STORAGE MODULUS (G'), FAM_HL.

SOURCE: AUTHOR.

FIGURE 22 - CURVES OF EXPERIMENTAL AND FITTED STORAGE MODULUS (G'), FAM_SS.

SOURCE: AUTHOR.

3.4 FRACTURE PROPERTIES OF FAM FAM_SS AND FAM_HL

As above mentioned, the non-linearity of the FAM studied herein was considered as a consequence of material microcrack growth and propagation. The CZ model selected in this study to model the damage evolution is based on the non-linear viscoelastic cohesive zone

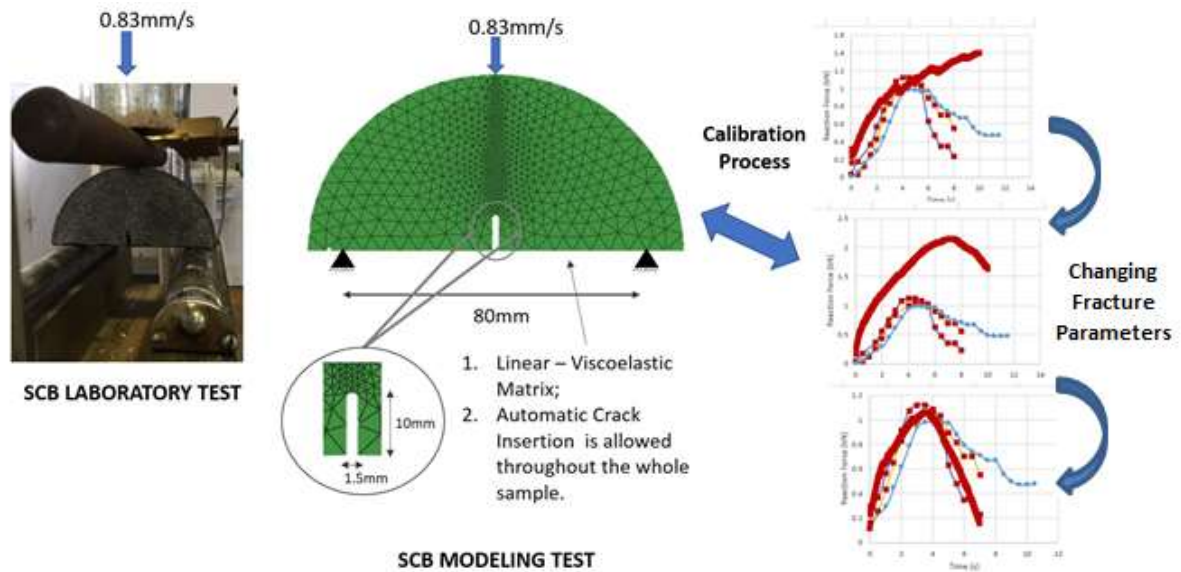
(NLVE-CZM) model developed by Allen and Searcy (2001), mathematically represented by Equation (7).

In order to perform the numerical simulations, one needs to obtain fracture parameters required in the adopted NLVE-CZM. For that, it was used herein a calibration procedure based on experimentally obtained fracture testing results. Some test configurations are being used to evaluate fracture characteristics of asphalt mixture: Single Edge Notch Beam (SENB); Disc-shaped Compact Tension (DCT); and Semi-Circular Bending (SCB) tests.

In this study, a semi-circular bend (SCB) geometry was selected for fracture testing. Given the various advantages such as repeatability, reproducibility, consistency, and simplicity of specimen preparation and testing, the SCB test has received a growing interest by the research community to characterize fracture properties of asphalt mixtures. According to Aragão (2011), SCB geometry has been used by many researchers (BASHAM et al., 1990; KHALID and ARTAMENDI, 2008; MOHAMMAD and LIECHTI, 2000; VAN ROOIJEN and de BONDT, 2008; LI and MARASTEANU, 2004 and 2010, and many more) to obtain fracture toughness, fracture energy, and stress-softening curves of various types of brittle and semi-brittle materials. Furthermore, the success in generating the requisite parameters for fracture assessment has ensued American and England research community in the development of SCB standard protocols (EN 12697-44:2010, AASHTO TP 105-13) under monotonic loading conditions (SASHA and BILIGIRI, 2015).

Thus, the SCB geometry was chosen in this study to obtain mode I fracture parameters. The calibration process is schematic represented in Figure 23.

FIGURE 23 - CALIBRATION PROCESS TO DETERMINE MODE I FRACTURE PARAMETERS.



SOURCE: AUTHOR.

3.4.1 SCB sample fabrication

The SCB samples were obtained from Marshall compacted specimens in laboratory. The target air void for that samples was (4,00 +/- 0,7 %), within the limit (3% to 5%) from bituminous mix design. Many attempts were made until the desired volume of voids was reached. At first by changing the Marshall compactor numbers of blows, and subsequently by changing the amount of mass inserted in the mold. Table 7 summarized volumetric parameters of SCB testing samples.

TABLE 7 - VOLUMETRIC PARAMETERS OF SCB TESTING SAMPLES.

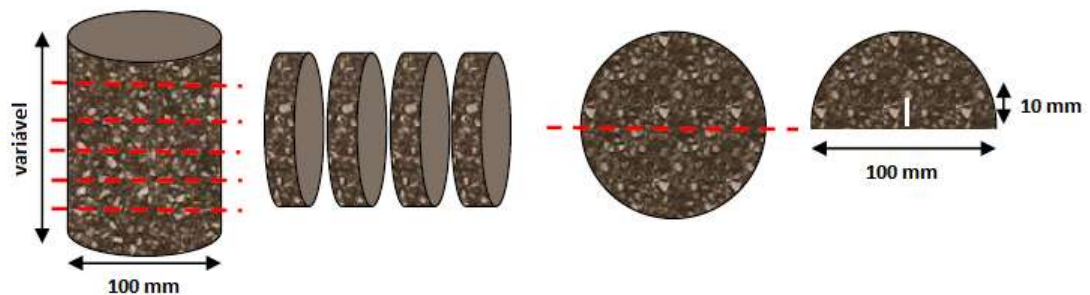
Filler	N° Blows	Diameter	Gmb	Gmm	Air Voids (%)
	p/ face	(mm)	(gr/cm ³)	(gr/cm ³)	
Steel Slag	75	10.2	2.22	2.318	4.17
Hydrated Lime	25	10.2	2.17	2.279	4.66

SOURCE: AUTHOR.

According to Gottardi (2015), who also studied these two fillers in HMA, the variation in the materials behavior (regarding air voids distribution) is expected as the average particle size of hydrated lime is 7 times lower than steel slag, being 10 μ m and 70 μ m, respectively. Figure 24 and Figure 25, shows the geometry and procedure, respectively, used herein to

obtain the semi-circular testing samples, with 100 mm of diameter, and a 10 mm notch made using 1.5mm blade along the axis of symmetry. The specimen thickness (25mm) adopted in this study was based on Aragão (2011). The author stated that for two-dimensional simulations, SCB specimens 25 mm thick can be used when it is assumed the plane stress condition.

FIGURE 24-ILLUSTRATION OF SCB SPECIMEN CORING AND CUTTING PROCEDURE.



SOURCE: ADAPTED FROM LUTIF (2011).

FIGURE 25 – ACTUAL SCB SPECIMEN CORING AND CUTTING PROCEDURE

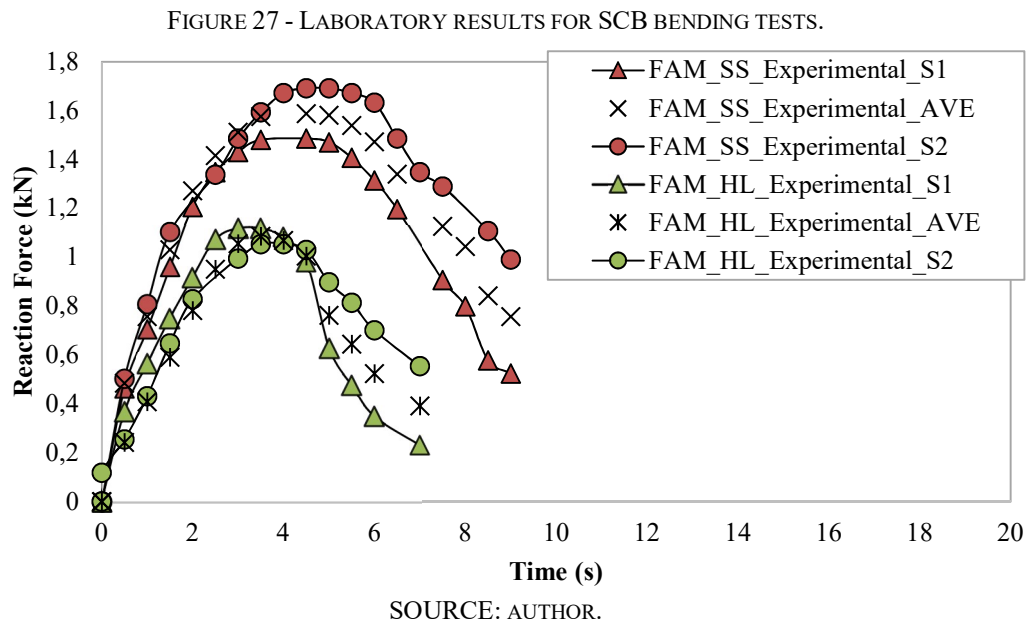


SOURCE: AUTHOR.

3.4.2 SCB experimental test and numerical calibration using MultiMech™ software

Two SCB samples for each studied FAM mixture were subjected to pure mode I SCB laboratory tests. Samples were loaded up to failure at a constant displacement rate of 0.83mm/s at $25 \pm 1^\circ$ C. The support's distance was fixed as 80 mm, as also used by Fonseca (2016), maintaining the same proportion of the SCB tests performed by Lutif (2011) and Aragão (2011) in bigger samples (using 150mm diameter) compacted in Superpave Gyratory

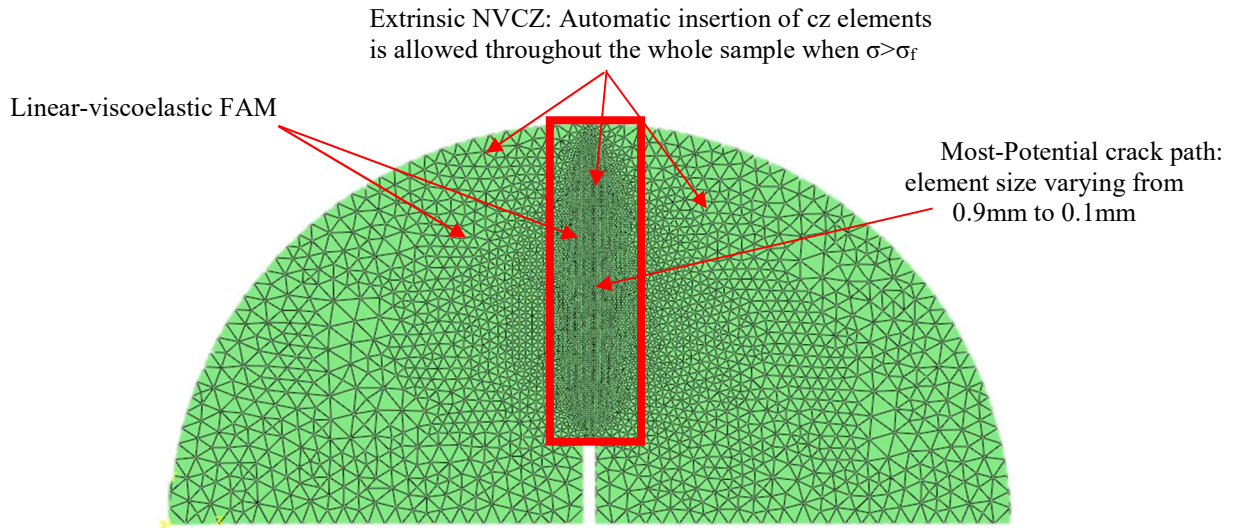
Compactor (80% of the sample diameter). The test set-up and execution are shown in Figure 26. SCB laboratory testing results are presented in Figure 27.



After performing SCB experimental tests, the calibration process was performed. For that, first a convergence study was conducted to identify the appropriate size of cohesive elements to model the SCB fracture testing. The FAM_HL mixture was used as reference for the convergence study. Six different meshes were simulated. The level of refinement was increased on the most potential cohesive zone area of SCB specimen, as shown in Figure 28. It was considered the following elements sizes: 0.9 mm, 0.7 mm, 0.6mm, 0.4mm, 0.2mm, and 0.1mm. The LVE material input properties used are the ones showed in Table 6. Since the effort is to investigate mesh convergence, for the cohesive zone fracture parameters,

arbitrarily values were used but with same magnitude as the ones used by Lutfi (2011) as show in Table 8.

FIGURE 28 – ILLUSTRATION OF SCB MESHING REFINEMENT



SOURCE: AUTHOR.

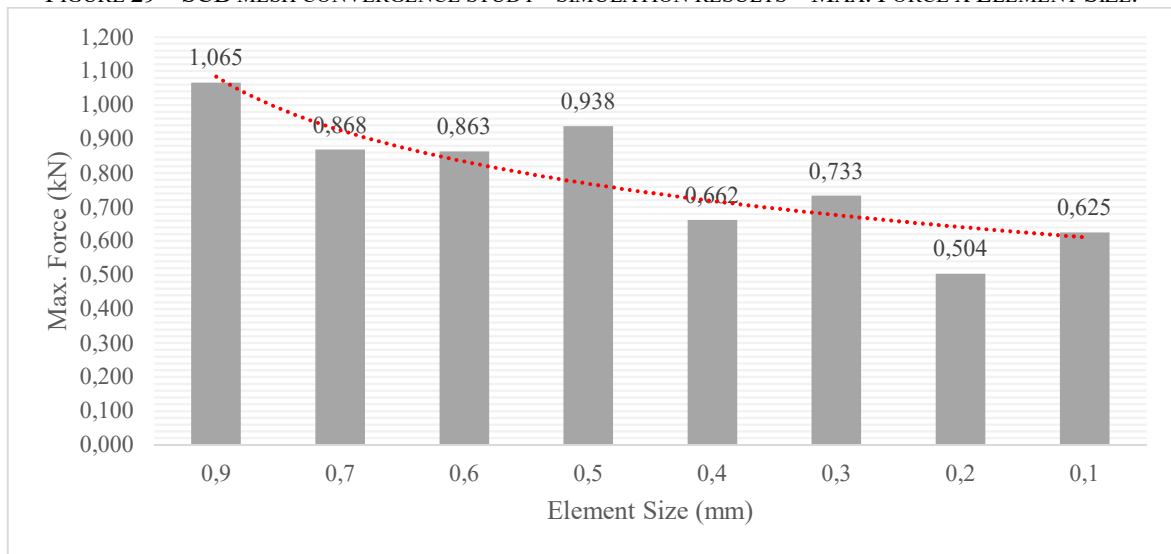
TABLE 8 - FRACTURE PARAMETERS USED FOR MESH CONVERGENCE STUDY.

FAM_HL			
δ_n^*	δ_s^*	55 mm	55 mm
σ_n^f	σ_s^f	9E+05 Pa	1.0E+20 Pa
	A		1E6
	m		3.4

SOURCE: AUTHOR.

Figure 29 shows the corresponding simulation results in the form of maximum reaction force vs. element size graphic. It can be observed considerable difference among the results due to changes in mesh refinement. Thus, an element size of 0.4 mm was chosen because was a fairly refined mesh with reasonable simulation computational time (14 time less than the size 0.2mm and 65 times less than 0.1mm).

FIGURE 29 – SCB MESH CONVERGENCE STUDY - SIMULATION RESULTS – MÁX. FORCE X ELEMENT SIZE.



SOURCE: AUTHOR.

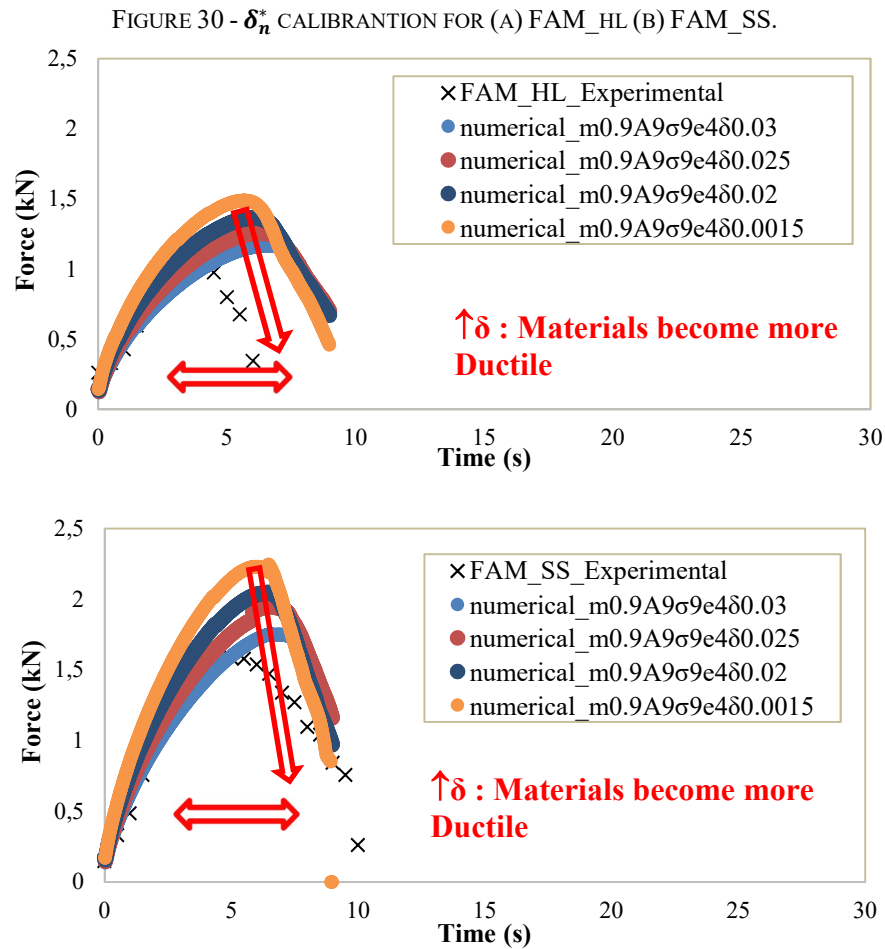
After de mesh convergence study, the mode I cohesive zone fracture parameters were determined by a trial-and-error calibration process, by varying fracture parameters from the Equation (7) until a good agreement between the experimental and numerical curves was obtained. Four parameters (δ_n^* , σ , m and A) of the NLVE-CZM were determined. The process of calibration, shown in Figure 23 accounts for the influence of each parameter in mixtures behavior. This is not a trivial task, since one needs to play with different set of parameters to obtain a matching curve. However, If one could understand the contribution of each parameter on the entire fracture process, the calibration can be conducted more efficiently by taking proper steps.

I think it is important to inform the reader that you used MultiMech to perform these numerical simulations.

- **Parameter δ^***

The first step in the calibration process was to define the parameter δ_n^* . From Allen and Searcy (2001), δ is the empirical material length parameter which reflect a length scale intrinsic to the scale of the damaged zone, representing the thickness of the cohesive zone. To determine the δ_n^* value, other parameters were fixed arbitrarily and δ_n^* was varied from 0.015

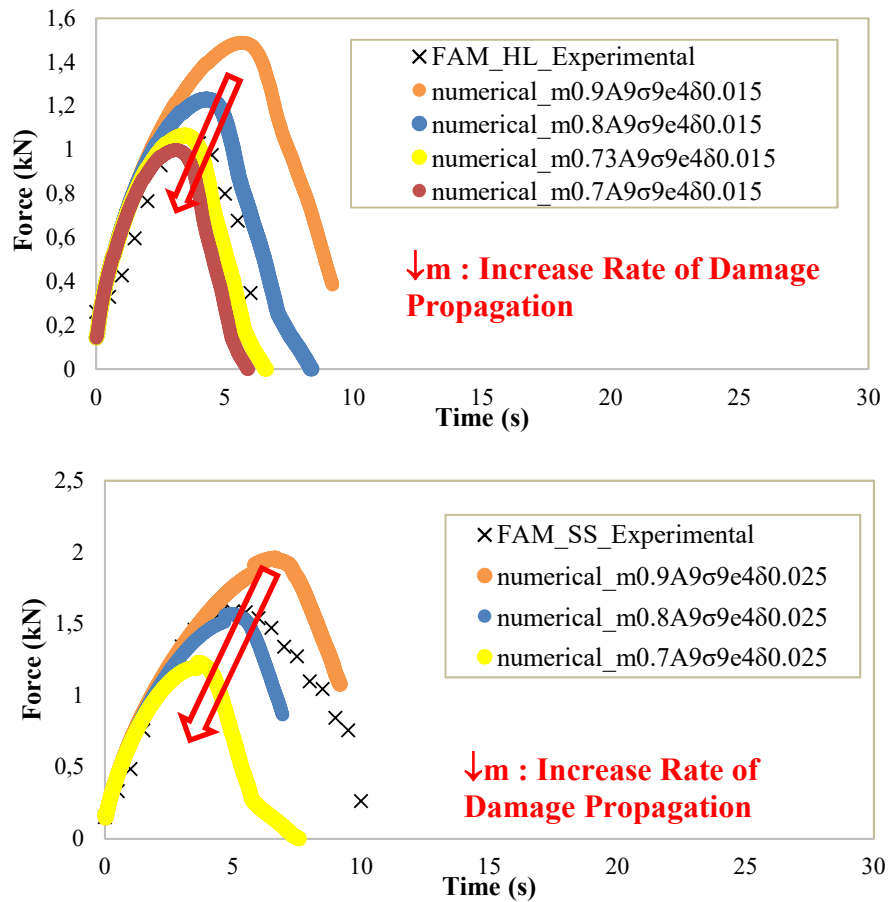
to 0.030 m. Results from Figure 30 indicate that δ_n^* changes the slope of the curve and peak, changing the entire fracture energy until sample failure. Therefore, if δ_n^* increases the more ductile the material becomes. The best fitted curve for FAM_SS was found with $\delta = 0.025$ and for FAM_HL was with $\delta = 0.015$.



SOURCE: AUTHOR.

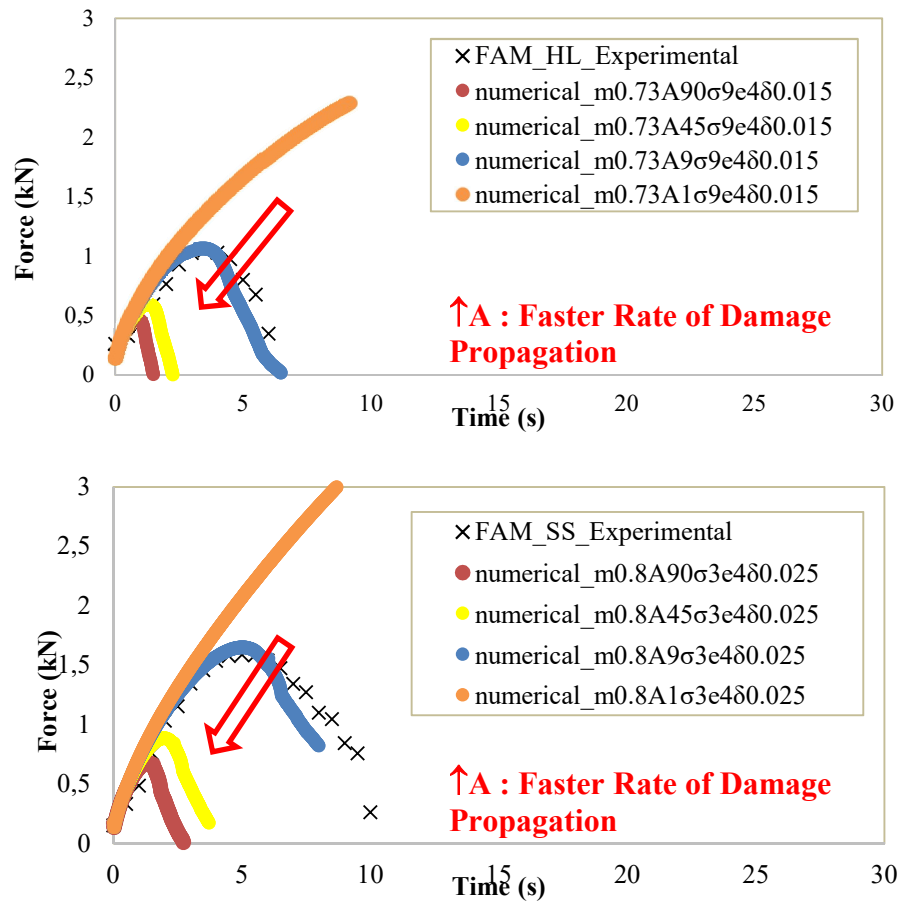
- **Parameter m and A**

The parameters A and m are used to define the internal damage evolution law, as stated in Equation (9), associated with the damage evolution rate which reflects a dependence on crack opening displacements and have a significant impact on the traction-displacement relationship. From Figure 31 is possible to observe that by decreasing the m parameter, the rate of damage propagation increases.

FIGURE 31 - m CALIBRANTION FOR (A) FAM_HL (B)FAM_SS.

SOURCE: AUTHOR.

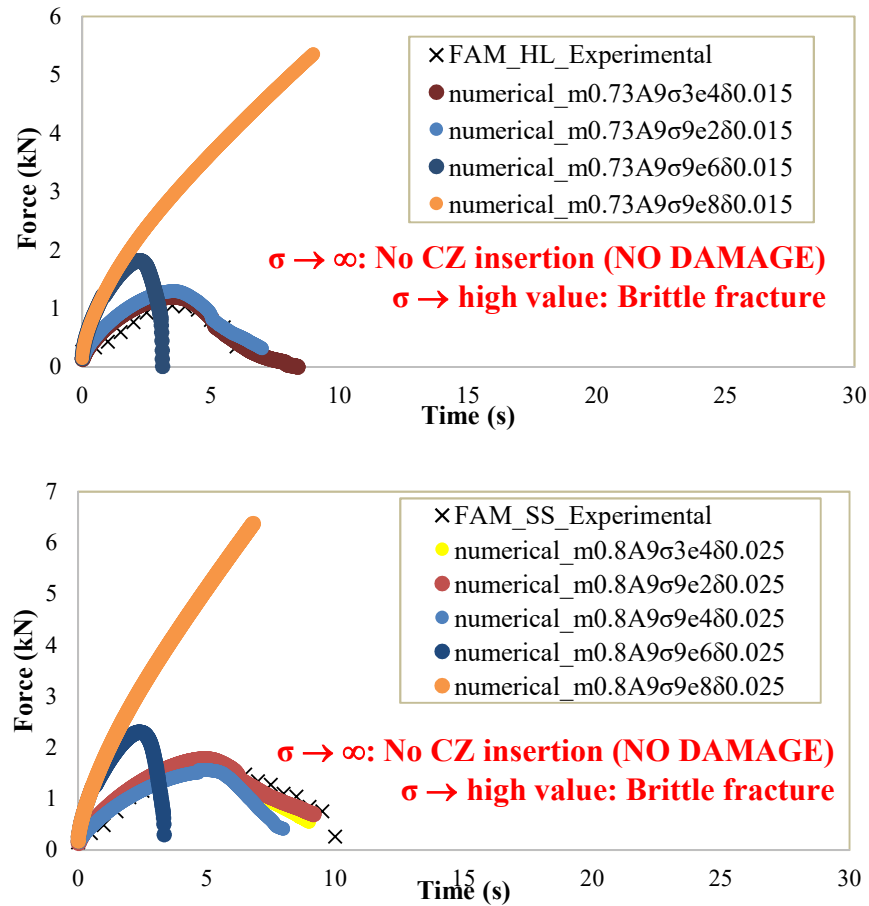
In contrast, from Figure 32 one can noticed that if A value is decreased the damage propagation in the material occurs more slowly. As the two parameters play the same role, first A was fixed and the best experimental-numerical match with different m values was obtained. Then, the inverse process was made to find the best match for A . An important observation must be made, the effect of m value is inversely proportional to the rate of damage propagation, since m was assumed herein to be less than 1. From Equation (9) it possible to explain that behavior, as the parameter m is an exponent of a variable smaller than 1.

FIGURE 32 - **A** CALIBRANTION FOR (A) FAM_HL (B) FAM_SS.

SOURCE: AUTHOR.

- **Parameter σ_f**

The last step to the fracture parameter's calibration is to find the magnitude of initial stress criteria, σ_f , requisite stress level to initiate damage. This is not a trivial task. However, from the current study, it is possible to observe that for higher values of σ_f , the fracture process occurs with lower energy absorption and at higher rate, characterizing a brittle fracture behavior, as shown in. If ones assume a $\sigma_f \gg 0$, physically, it means that the CZ initiation criteria is never reached, and material will never failure due to fracture. Figure 34 shows the final curves of calibrated numerical results and the averaged experimental results for both mixtures.

FIGURE 33 - σ_f CALIBRATION FOR (A) FAM_HL (B)FAM_SS.

SOURCE: AUTHOR.

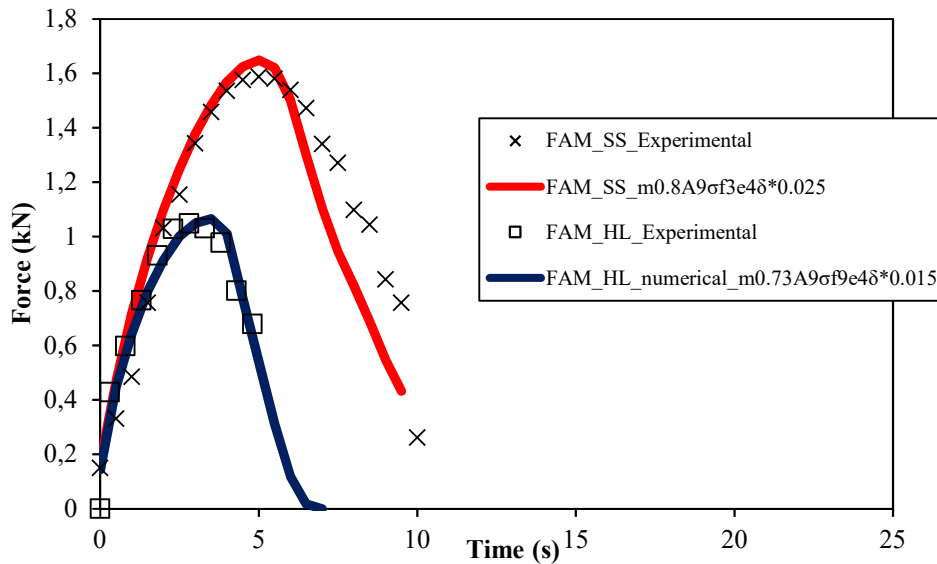
Finally, Mode II cohesive zone fracture parameters were defined with high σ values and the same δ determined for Mode I. This because in the test used herein to validate the model the fracture process occurs essentially by traction (mode I), well detailed below, then high values of σ were defined in order not to create CZ by mode II. About δ , it was defined with same value of mode I parameter just because it cannot be zero as it is a denominator in Equation (8), and its value does not interfere in Equation (7) result as we do not have fracture by mode II. Table 9 summarizes the input material parameters obtained with the methodology employed herein for the mixtures studied (FAM_HL and FAM_SS).

TABLE 9 – LVE MATERIAL PROPERTIES (PRONY SERIES) AND NLVE-CZM FRACTURE DAMAGE PARAMETERS FOR MODEL SIMULATIONS.

FAM mixtures	FAM HL	FAM SS
Laboratory tests and target model inputs	(1) Dynamic frequency sweep test using FAM specimens: linear viscoelastic material properties (Prony series parameters in the generalized Maxwell model) (2) Semi-circular bending test using FAM specimens: cohesive zone fracture parameters	
Test results (model inputs)	(1) Linear viscoelastic properties (Prony series parameters)	
	E_1 9.39 E+09 Pa	5.23E+09 Pa ρ_1 1.10E-04
	E_2 7.04 E+08 Pa	1.95E+09 Pa ρ_2 1.10E-03
	E_3 4.91 E+09 Pa	5.83E+09 Pa ρ_3 1.10E-02
	E_4 4.68 E+08 Pa	4.41E+08 Pa ρ_4 1.10E-01
	E_5 2.19 E+08 Pa	2.60E+08 Pa ρ_5 1.10E+00
	E_6 6.56 E+07 Pa	6.01E+07 Pa ρ_6 1.10E+01
	E_7 3.93 E+07 Pa	7.70E+07 Pa ρ_7 1.10E+02
	E_8 1.24 E+07 Pa	1.89E+07 Pa ρ_8 1.10E+03
	E_∞ 4.10 E+07 Pa	7.70 E+07 Pa
	(2) Nonlinear viscoelastic cohesive zone parameters	
	δ_n^* 0.015 m	0.025 m
	σ_n^f 9.0 E+04 Pa	3.0 E+04 Pa
	A 9	9
	m 0.7	0.8
Properties assumed	ν 0.3	0.3
	Mode I (normal) and mode II (shear) cohesive material length parameter δ_i^* is assumed to be equal in this study, and Mode II (shear) initial stress level σ_s^f is assumed to be 2.3E+7 (very high) to eliminate mode II CZ.	

SOURCE: AUTHOR.

FIGURE 34 – MODE I FRACTURE PARAMETER AFTER CALIBRATION.



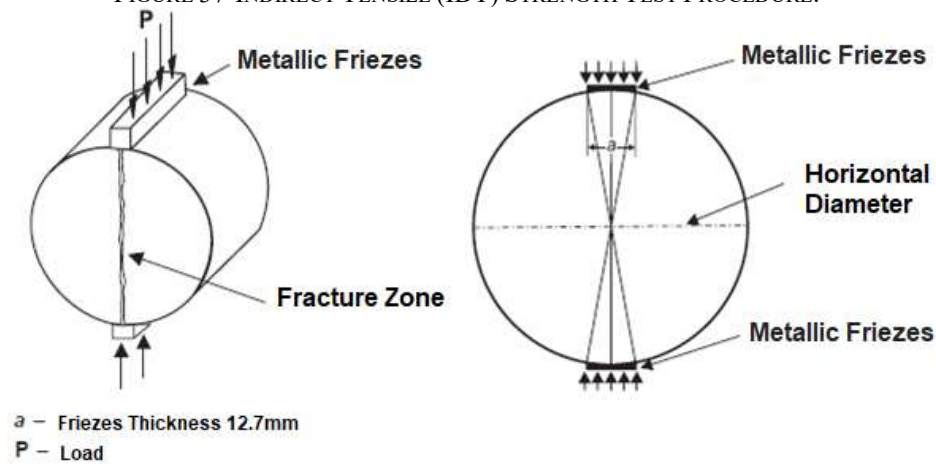
SOURCE: AUTHOR.

3.5 INDIRECT TENSION STRENGTH TEST (IDT)

As is widely known, concrete has a tensile strength much lower than compressive strength. The tensile strength is an important characteristic for asphalt mixtures since pavements experience high tensile strains in the bottom of the surface layer when traffic load is applied on its top. If the material does not have sufficient tensile strength, it starts to develop cracks, and consequently is a critical factor in pavements design life. Thus, the tensile strength has been shown to be an important parameter for the characterization of asphalt mixtures.

The so-called Brazilian test for evaluating tensile strength in concrete materials is by diametrical compression mode. For this reason, it is known as indirect tension test (IDT). It was developed by professor Lobo Carneiro in Rio de Janeiro, Brazil (CARNEIRO, 1943). The test configuration considers the application of two concentrated and diametrically opposed forces of compression in a cylinder (Figure 37). Uniform tensile stresses perpendicular to the diameter are generated. Since 1972, this testing procedure has been used in bituminous mixtures characterization (BERNUCCI, 2006), including the American standard ASTM D6931. Authors have been using the IDT to evaluate asphalt mixtures performance due its ease and quick execution and fabrication of replicates (ZHANG et al., 2016; TUAN NGUYEN, 2013).

FIGURE 37-INDIRECT TENSILE (IDT) STRENGTH TEST PROCEDURE.



SOURCE: ADAPTED FROM BERNUCCI (2006).

In IDT tests for asphalt mixtures, the Marshall specimen is loaded through a 12.7 mm thick metallic strips (Figure 37). The Brazilian and American standards, DNIT 136 (2010) and ASTM D 6931, respectively, do not consider the influence of these strips in the tensile strength determination. According to the expression used by these entities, only the elastic behavior of the materials is taken into account and the rupture of the specimen along the requested diameter are due solely to the uniform tensile stresses generated. The IDT tension strength T_{IDT} can be determined as follows:

$$T_{IDT} = \frac{2 \cdot P}{\pi \cdot D \cdot l} \quad (11)$$

Where,

T_{IDT} : the indirect tensile strength;

P : the peak applied force;

D : the diameter of Marshall specimen;

l : the thickness of concrete specimen.

Considering the importance as a structural indicator for asphalt concrete resistance, for validation of the computational microstructure model, IDT tests were conducted. Marshall specimens were mold for the two FAM mixtures studied herein. To use the input properties

determined from frequency sweep and SCB tests in the numerical simulations of IDT, same mix design and procedures described in 4.4.1 are adopted. table 10 the volumetric parameters for the two samples compacted for IDT tests.

TABLE 10 - MARSHALL TESTING SAMPLES VOLUMETRIC PARAMETERS FOR IDT TESTS.

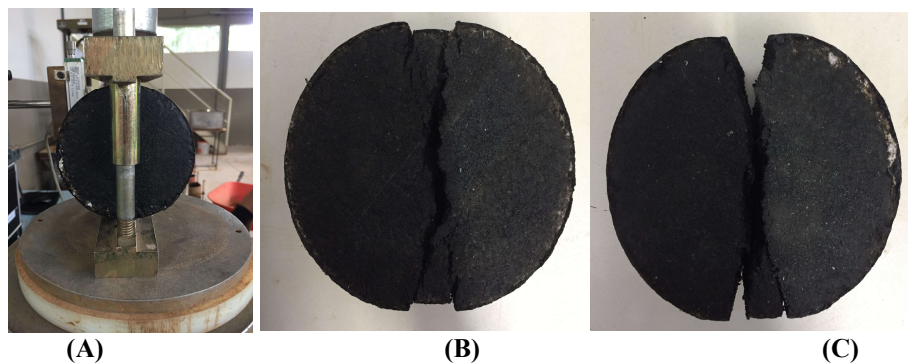
	Blows N°	Diâmeter (cm)	Dry Mass (gr)	Gmb (gr/cm ³)	Gmm (gr/cm ³)	Vv (%)
FAM_HL	25	10.2	1111.10	2.181	2.318	4.33
FAM_SS	75	10.2	1331	2.259	2.279	2.49

SOURCE: AUTHOR.

3.5.1 IDT experimental setup and results

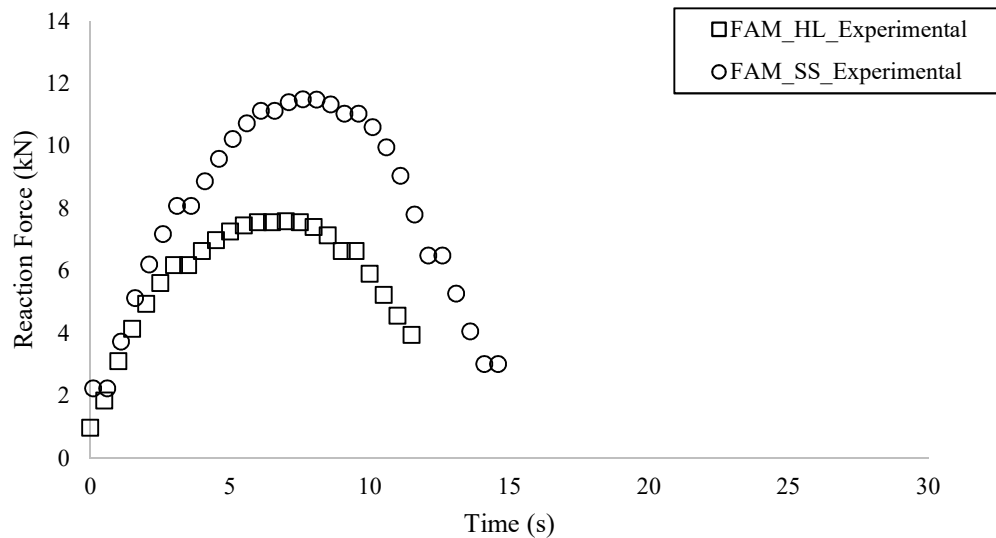
IDT was conducted on 10cm diameter and 6.2cm thick Marshall specimens of the studied FAM mixtures at a testing temperature of 25 °C. Samples air voids were maintained at $4 \pm 0.5\%$. A monotonic constant displacement rate of 0.83mm/s was applied to the top center point until the specimens failed completely. Test results, plotting the reaction forces captured by the load cell as the loading time increased, were used for the validation of the model, by comparing experimental and numerical results. Figure 35 shows the experimental setup for the test and the FAM specimens (after being tested) with a macrocrack developed at the center region. The laboratory test results are shown in Figure 36.

.FIGURE 35 – (A) IDT SAMPLE SETUP. (B) FAM_HL AND (C) FAM_SS AFTER TEST.



SOURCE: AUTHOR.

FIGURE 36 - LABORATORY RESULTS FOR IDT STRENGTH.



SOURCE: AUTHOR.

4. VERIFICATION AND VALIDATION OF MICROSTRUCTURE NUMERICAL MODEL

To verify the model used herein to evaluate bituminous mixtures, first it was performed some trial simulations of a tapered bar problem with known analytical solution to verify the material models available in MultiMechTM software.

The initial simulations included: (I) an elastic model without damage verification; and (II) a viscoelastic model without damage verification. After the verification, the IDT Strength Test was simulated, and results were compared to experimental ones obtained previously.

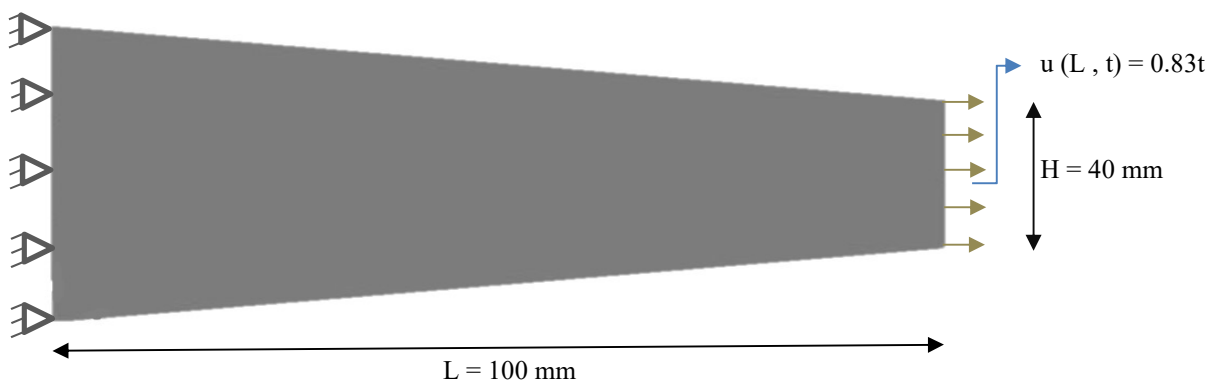
4.1 VERIFICATION OF ELASTIC CONSTITUTIVE MODELS WITHOUT DAMAGE

In this first attempt, a closed-form solution problem was solved in order to verify the efficiency and accuracy of the MultimechTM algorithms and optimizer. Thus, numerical results from MultimechTM were compared to numerical results from Abaqus for the same problem. Thus, a homogeneous tapered bar problem, presented in FIGURE 37, was used. The

tapered bar was assumed with elastic materials and monotonically increasing displacements were applied at the right end of the bar.

The tapered bar problem was selected because of its inhomogeneous state of stress (as a result of its varying cross-section along the bar), which allowed the verification of different stress behavior along the bar. Table 11 presents the material properties used that were arbitrarily assumed for comparison purposes only.

FIGURE 37 - ELASTIC TAPER BAR PROBLEM.



SOURCE: AUTHOR.

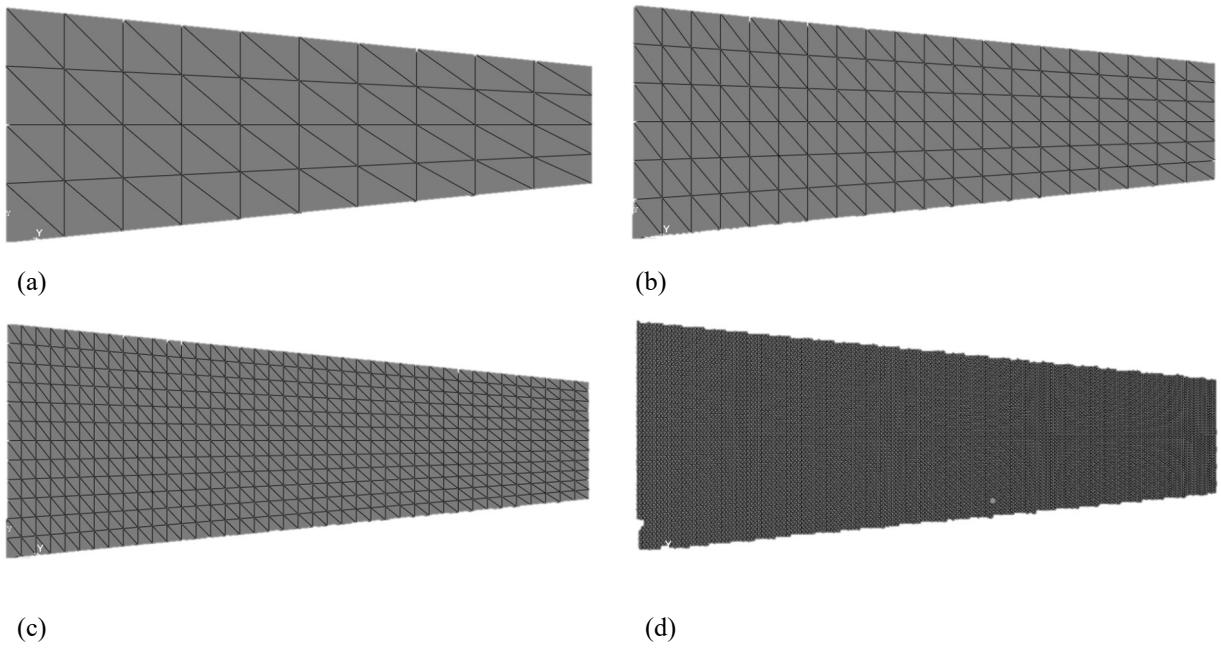
TABLE 11- MATERIAL PROPERTIES FOR THE ELASTIC TAPERED BAR USED FOR THE ELASTIC MODEL VERIFICATION.

ISOTROPIC LINEAR ELASTIC	
Young Modulus (E)	122000
Poisson Ratio (ν)	0.35

SOURCE: AUTHOR.

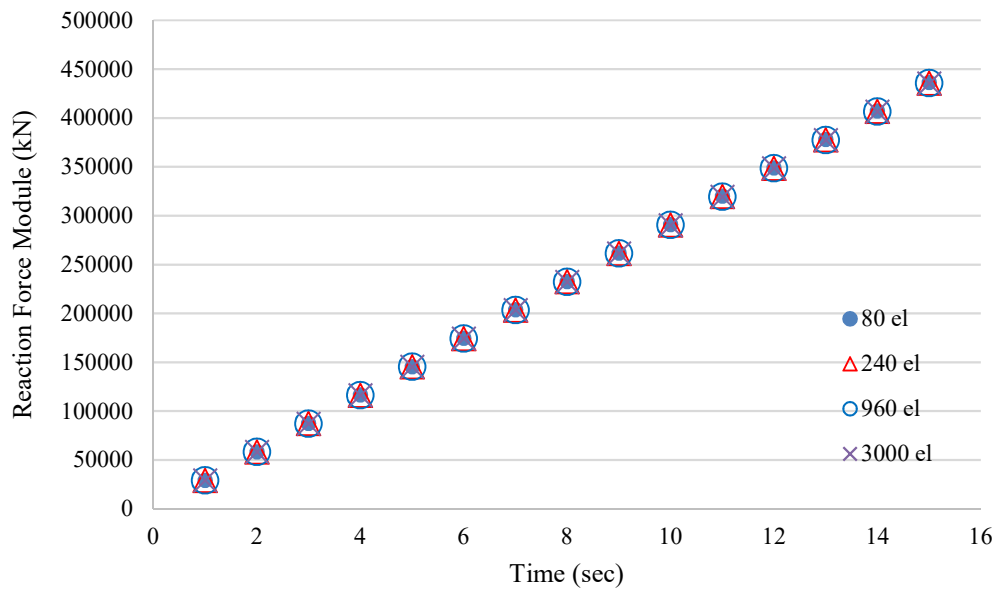
A convergence study was first conducted to identify the appropriate finite element mesh of the global scale object to model the tapered bar. Four different meshes in different level of refinement (80, 240, 960, 3000 elements) were investigated. Figure 38 shows the four meshes generated for this study and Figure 39, the corresponding simulation results in the form of Reaction Force (kN) vs. Time (sec) graphics. According to graphic analyses, the level of refinement did not affect the solution, which implied that 80 global elements were enough to obtain converged solutions for this problem. Thus, the mesh with 80 elements was chosen for the remaining simulations as it reduces the simulation time.

FIGURE 38 – TAPERED-BAR MESH CONVERGENCE STUDY FOR FOUR MESH REFINEMENT ELEMENT NUMBER: (A) 80 ELEMENTS; (B) 240 ELEMENTS; (C) 960 ELEMENTS; (D) 3000 ELEMENTS.



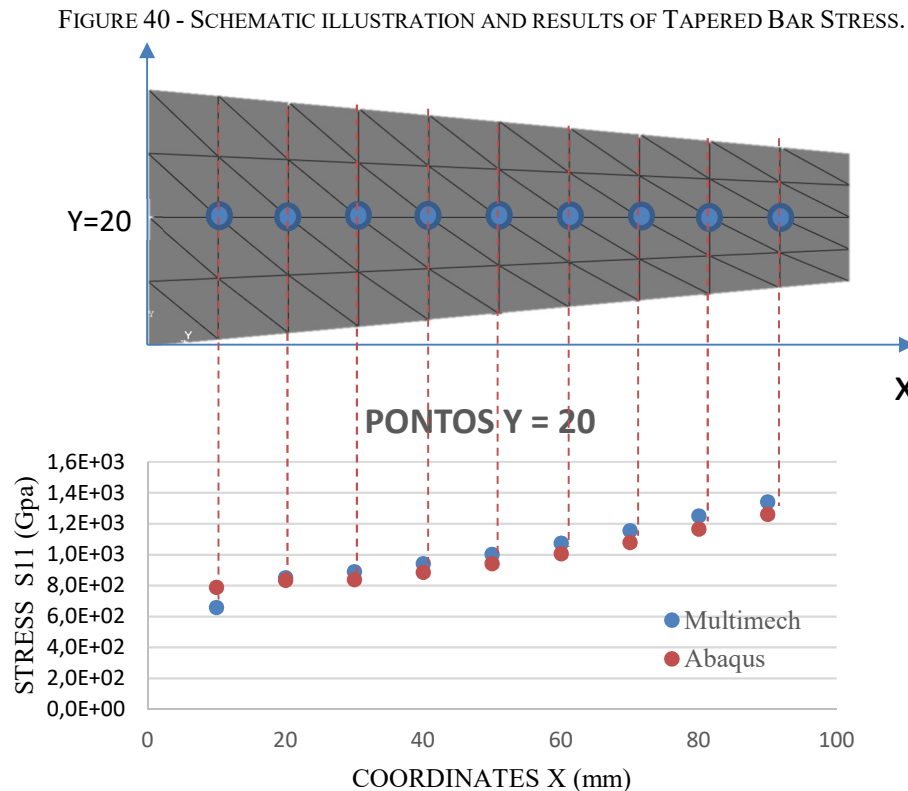
SOURCE: AUTHOR.

FIGURE 39 – TAPERED BAR MESH CONVERGENCE STUDY - MULTIMECH SIMULATION RESULTS.



SOURCE: AUTHOR.

Simulation results from Multimech can be compared to results from ABAQUS. The comparison was made by the stress value (S11) in some specific points. Figure 40 illustrate the points used in the verification their respective stress results from Multimech and Abaqus.

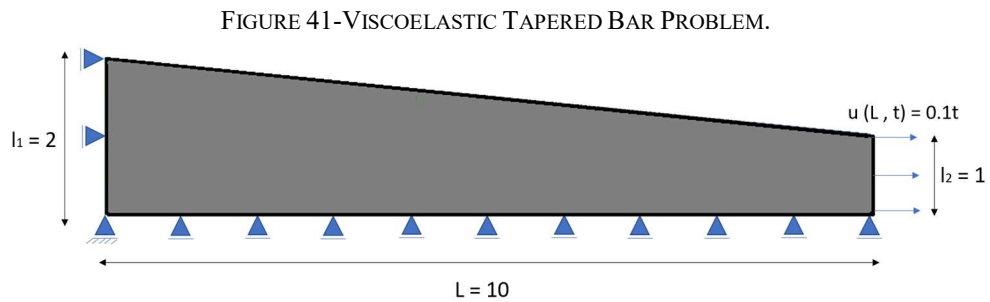


SOURCE: AUTHOR.

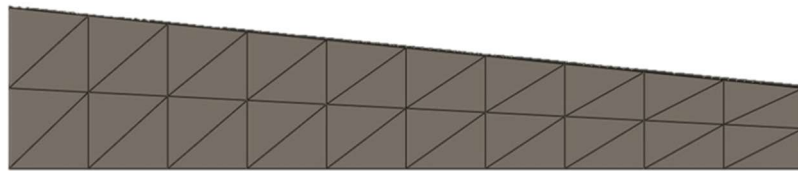
Figure 40 shows that the numerical simulation results from both softwares are close. The difference between these stress results from Abaqus and Multimech is about 8% and can be explained by the fact that Multimech gives interpolated stress values between elemental stresses that contains that specific analyzed point, while Abaqus do not interpolate the stress values and the stress are given per element. In this study, to obtain Abaqus results for comparison, one element connected to a specific analyzed point was randomly selected without interpolation.

4.2 VERIFICATION OF VISCOELASTIC CONSTITUIVE MODEL WITHOUT DAMAGE

The second attempt to verify the model was with a viscoelastic problem. For this purpose, another closed-form solution problem was solved, but at this time, the numerical results are compared to analytical solutions. Due to the axis of symmetry, only half of the bar was modelled, the geometry and boundary conditions used to the problem are shown in Figure 41.



(a) Tapered Bar Geometry and Boundary Conditions.



(b) Global scale mesh with 40 elements.

SOURCE: AUTHOR.

The tapered bar material was assumed as a viscoelastic matrix. The material properties used to characterize the tapered bar were arbitrarily selected based on other studies and are presented in Table 12.

TABLE 12- MATERIAL PROPERTIES USED FOR VISCOELASTIC VERIFICATION.

E_{∞}	1.22E+07 Pa		
ν	0.35		
E_1	3.03E+09 Pa	ρ_1	8.00E-05
E_2	1.48E+09 Pa	ρ_2	8.00E-04
E_3	1.33E+09 Pa	ρ_3	8.00E-03
E_4	4.35E+08 Pa	ρ_4	8.00E-02
E_5	1.60E+08 Pa	ρ_5	8.00E-01
E_6	5.00E+07 Pa	ρ_6	8.00E+00
E_7	1.79E+07 Pa	ρ_7	8.00E+01
E_8	3.02E+06 Pa	ρ_8	8.00E+02

SOURCE: AUTHOR.

The analytical solution for this problem is given by:

$$\bar{E}(t) = E_{\infty} t + \sum -E_i \rho_i e^{\frac{-t}{\rho_i}} + \rho_i E_i \quad (12)$$

$$\varepsilon(x, t) = \frac{0.1t}{\ln(2)} \left(\frac{1}{20-x} \right) \quad (13)$$

$$\sigma(x, t) = \frac{0.1}{\ln(2)} \left(\frac{1}{20-x} \right) E(t) \quad (14)$$

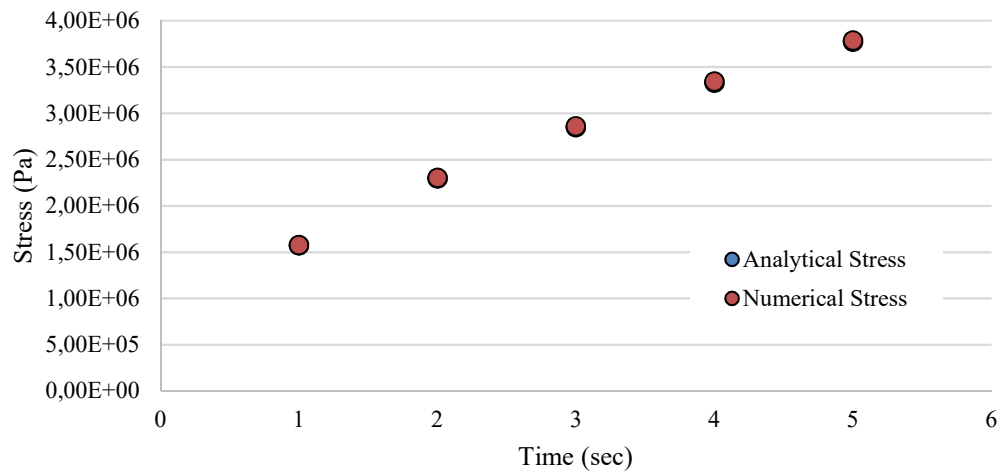
The results from analytical solution were compared with results from MultiMech numerical simulation by stress values in one specific point, coordinates (0,1), on the tapered bar. Table 13 and Figure 42 show the results and comparisons.

TABLE 13 – STRESS VALUES FROM ANALYTICAL AND MULTIMECH ANALYSIS.

STRESS S11				
Point	Time	Analytical Stress (Pa)	Multimech Stress (Pa)	Variation
(0,1)	1	1573991.82	1579543.026	0.35268%
	2	2298414.23	2306520.359	0.35268%
	3	2851407.72	2861464.163	0.35268%
	4	3333209.79	3344965.465	0.35268%
	5	3775014.53	3788328.376	0.35268%

SOURCE: AUTHOR.

FIGURE 42 - STRESS VALUES FROM ANALYTICAL AND MULTIMECH ANALYSIS AT THE POINT (0, 1) ON THE TAPERED BAR.



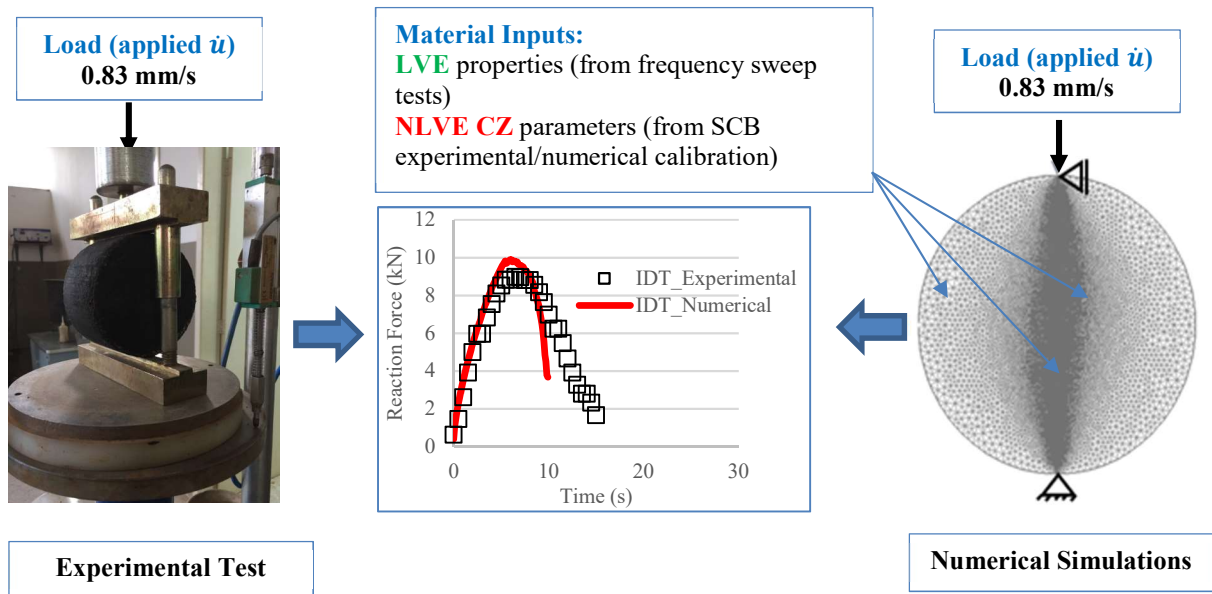
SOURCE: AUTHOR.

From Table 13 and Figure 42, it can be observed that the values are extremely close with difference under 0.5%, demonstrating the efficacy and accuracy of numerical model used herein to evaluate the behavior of viscoelastic materials subject to monotonic loading conditions.

4.3 VALIDATION OF THE MICROSTRUCTURE MODEL CONSIDERING DAMAGE

The verifications described above do not take in account the cohesive zones due to damage of the material. The effectiveness of the model for damage-induced problems was verified by simulating the IDT described in 4.5. Test results, plotting the reaction forces captured by the load cell as the loading time increased, were used for the validation of the model, by comparing experimental and numerical results. Figure 43 shows the overall methodology employed to validate the model used herein, including boundary conditions imposed.

FIGURE 43 - SCHEMATIC ILLUSTRATION OF METHODOLOGY EMPLOYED FOR MODEL VALIDATION.

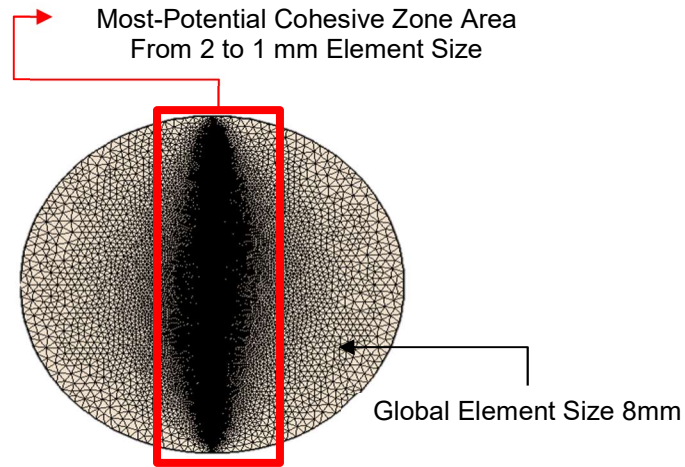


SOURCE: AUTHOR.

4.3.1 Mesh Convergence Study for IDT Strength Test Validation

Prior to performing the validation simulations, a mesh convergence study was conducted for the IDT testing geometry to ensure that a correct level of refinement was applied. Six different meshes were investigated, with the elements sizes on the most-potential cohesive zone area of 2mm (4896 el.), 1.7mm (6132 el.), 1.5mm (7230 el.), 1.2mm (10052 el.), 1.1mm (11428 el.), and 1mm (13096 el.). Figure 44 shows the refinement level procedure used. For the convergence study, arbitrary fracture parameters were used.

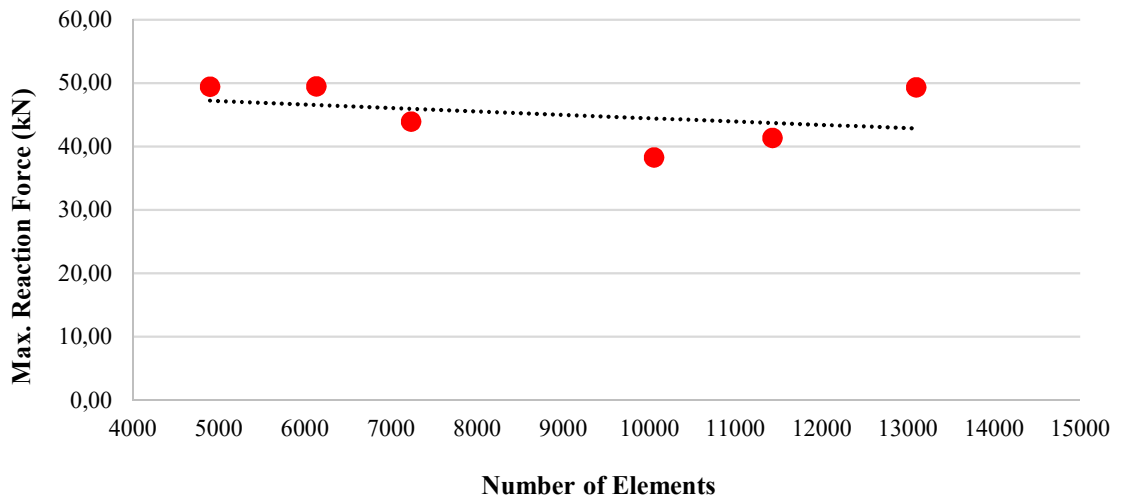
FIGURE 44 – IDT STRENGTH TEST MESH CONVERGENCE STUDY FOR COHESIVE ELEMENT SIZES.



SOURCE: AUTHOR.

FIGURE 45 shows the maximum reaction force vs. n^o of elements. Even though there was no considerable difference observed in the results, the element size of 1.0 mm was chosen because was the most refined mesh but with still a reasonable computational time.

FIGURE 45 – IDT MAX. REACTION FORCE VS. NUMBER OF ELEMENTS.



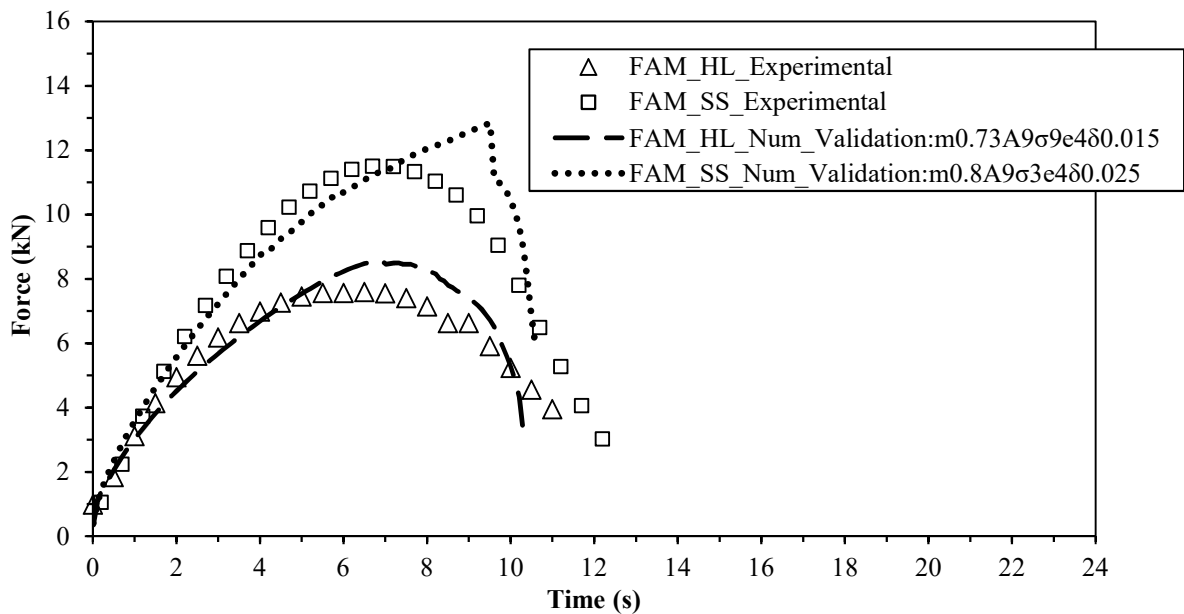
SOURCE: AUTHOR.

4.3.2. Validation of IDT Strength Test with Damage

To investigate the initiation and propagation of cracks in asphalt pavements it is necessary to insert damage evolution laws in the model. FAM mixtures were modeled as

isotropic linear viscoelastic with discrete fracture by NLVE-CZM. The linear-viscoelastic properties and non-linear viscoelastic cohesive zone parameters were experimentally obtained and defined in Table 9. Figure 46 show a comparison among numerical simulations with experimental results.

FIGURE 46 - TEST RESULTS VS. MICROSTRUCTURE MODEL SIMULATION RESULTS OF FAM BITUMINOUS MIXTURE: IDT VALIDATION.



SOURCE: AUTHOR.

As shown in Figure 46, the initial slope from numerical simulations matched well with the experimental results, which demonstrates that, along with the appropriate constitutive model, the linear-viscoelastic material properties used were well determined. Also, for FAM_HL, even before taking any calibration of damage parameters, a fair agreement between experimental and numerical simulation results is observed which indicates that the rate-dependent fracture parameters were also well determined for that mixture. In contrast, for FAM_SS, after 5 seconds, the moment when the reaction force in the experimental curve started to gradually decrease due to significant damage, the numerical result did not match well with the experimental data.

The difference in FAM_SS experimental and numerical results could be associated with mode II fracture. Since this mixture presented more ductile behavior (higher delta) than FAM_HL, and more CZ elements were developed within the sample, it could be more prone to mode II fracture mechanics that was not considered in the analysis.

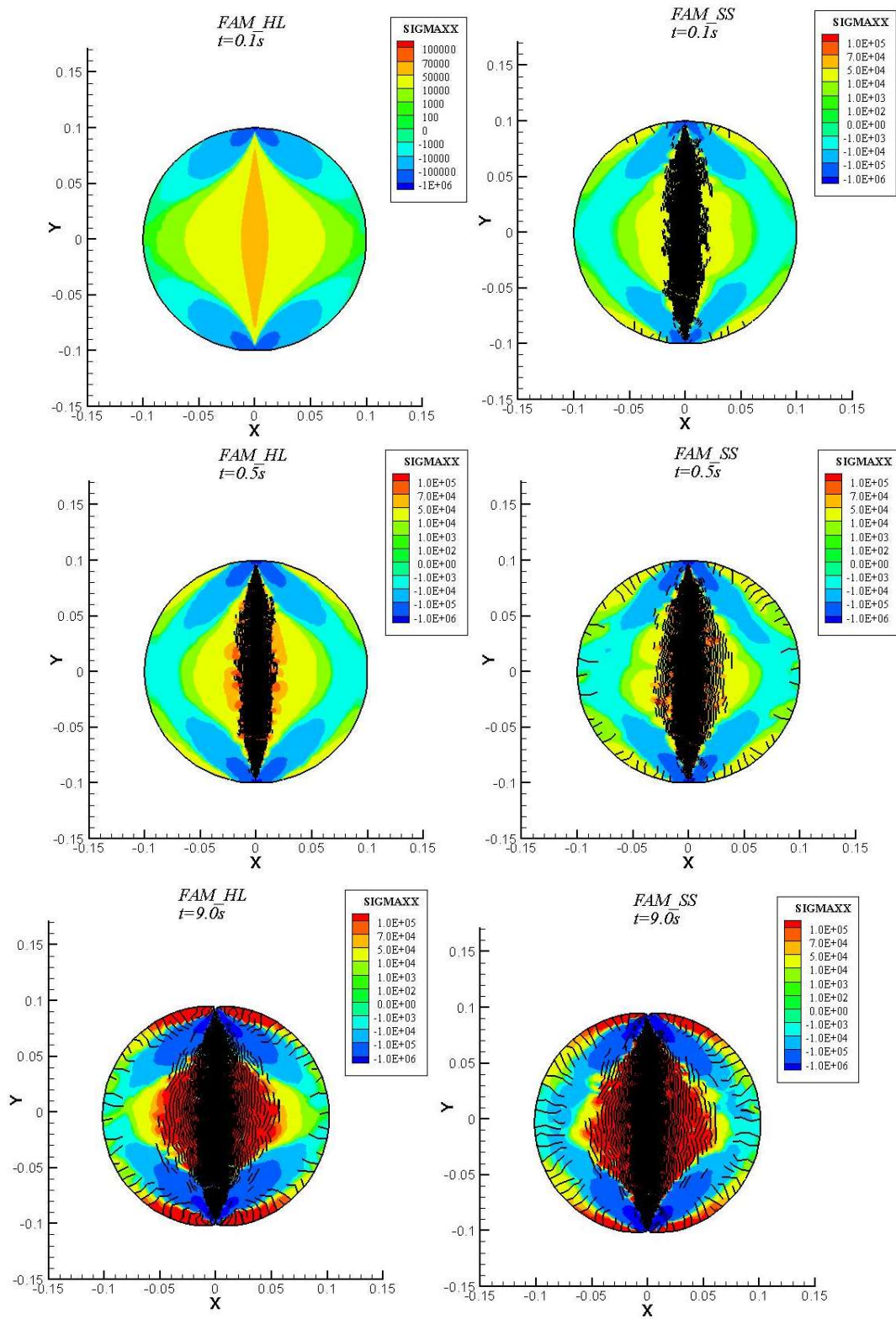
Further observations through the computational modeling can be made by visualizing the deformed mesh and elemental stress contours as shown in Figure 47. As expected in IDT tests, tensile stresses are developed diametrically opposed to the loading direction while compressive stresses are observed at the supports.

Observing the FAM_HL, the following cracking evolution was obtained: at about 0.5 seconds, the CZ initial stress level is reached at the higher tensile stress region (at the center of the specimen) and CZ elements are inserted in the finite element mesh. Note that this does not mean that cracks are developed in the sample yet. It can be observed some tensile stress concentration at the center with cohesive elements, but stress values continue to increase. At 9 seconds, the tensile stresses start to decrease, meaning that microcracks were developed and alleviated those stress concentration regions. At 10 seconds, there is no more tensile stress and after that, a macrocrack can be observed.

As for the FAM_SS, the first CZ elements (potential region of cracks) are inserted at 0.1 seconds. Tensile stresses keep increasing until approximately 10 seconds, with no microcrack developments observed in the material. FAM_SS only failures at approximately 13 seconds. Although the CZ elements are inserted earlier in FAM_SS than FAM_HL, in a certain way CZ elements relieve the stresses in the FAM, so the mixture resist to higher loads without abruptly breaking, showing a more ductile material behavior. These findings corroborate with experimental results from Fonseca (2016). The author used time sweep tests to evaluate material integrity due to damage accumulation based on damage characteristic

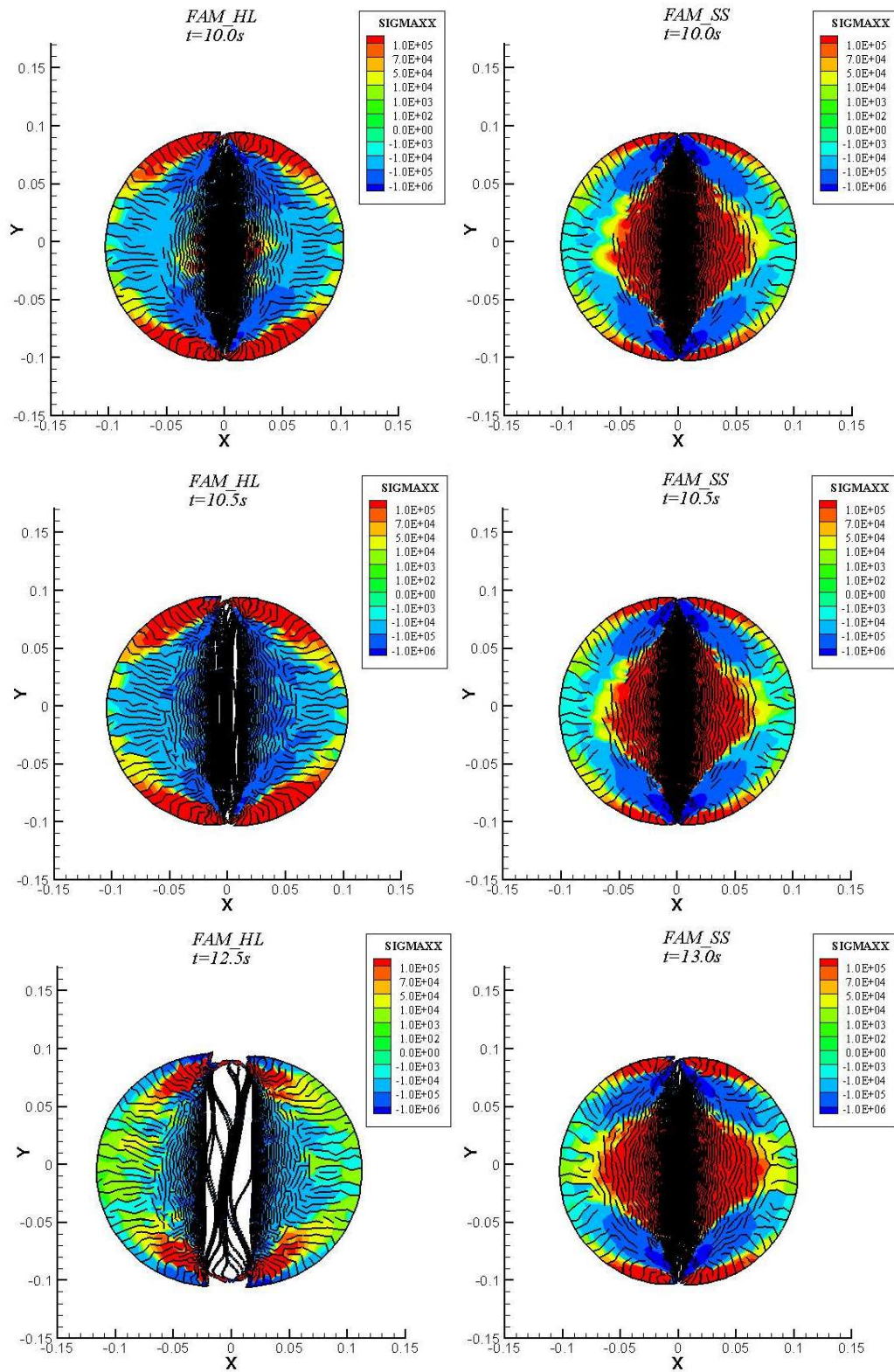
curves derived from Simplified Viscoelastic Continuum Damage (S-VECD) model. FAM_HL shows a lower integrity than FAM_SS at the same level of damage accumulation, which means a lower tolerance to fatigue damage than FAM_SS.

FIGURE 47 - DEFORMED MESH AND LONGITUDINAL STRESS CONTOURS BEFORE MICROCRACKING INITIATION AT DIFFERENT LOADING TIMES.



SOURCE: AUTHOR

FIGURE 48 - DEFORMED MESH AND LONGITUDINAL STRESS CONTOURS AFTER MICROCRACKING INITIATION UNTIL COMPLETE FAILURE AT DIFFERENT LOADING TIMES.



SOURCE: AUTHOR

In sum, from experimental results, it can be noticed that FAM_HL fails first than FAM_SS. This observation can be related to the NVCZ parameters. FAM_HL model has a lower value of m , which implies in greater rate of damage propagation. However, σ^f are higher to FAM_HL, indicating this mixture is more resistant to crack initiation. The higher peak value obtained by FAM_SS may be more related to material initial stiffness, since the linear viscoelastic parameters obtained were slightly higher. The higher stiffness of FAM_SS also resulted in lower σ^f , developing CZ earlier. Even though FAM_SS presented initial CZ areas first, it resists more to microcracking formation due to its ductile behavior (higher δ_n^*).

After the verifications and validation, the numerical results obtained using the model showed to be efficiently and accurately enough to predict the damage-dependent behavior of the bituminous composites with hydrated lime specimens used herein and the influence of the filler could be assessed. About the bituminous composites with steel slag, some adjustments must be made to calibrate the model, however we already could evaluate the influence of the steel slag in the mixtures with the model found herein.

5. CONCLUDING REMARKS

The main goal of this study was to employ a microstructure numerical modelling technique to assess the influence of different fillers in the behavior of FAM mixtures. With that, one could verify the potential of different materials (such as steel slag herein) to be incorporated in asphalt mixtures.

Analysis of the linear-viscoelastic properties of the studied FAM mixtures and fracture parameters were performed, and a nonlinear viscoelastic cohesive zone model (NVCZ) was used for predicting the damage-dependent mechanical behavior of FAM bituminous composites with different filler addition.

FAM mixture performance with steel slag filler and or hydrated lime addition were evaluated by FAM analysis and the matrix properties required as input for the computational model were obtained from simple laboratory tests. The linear viscoelastic properties of matrix were obtained by dynamic frequency sweep tests and represented by Prony series. The non-linear viscoelastic fracture characteristics of the matrix was considered by employing a micromechanically based non-linear rate-dependent viscoelastic cohesive zone model (NLVE-CZM) and simulations of experimental fracture tests (SCB) were carried out to calibrate the rate-dependent fracture parameters. With that, analysis of the influence of each fracture parameter on the behavior of the mixture was performed.

Some attempts have been made to verify the model algorithm used herein to evaluate bituminous mixtures, therefore problems with closed-form solutions were used comparing numerical and analytical results. The results show the efficiency and accuracy of the numerical model to evaluate problems involving elastic and viscoelastic material. To validate the model, indirect tensile strength test (IDT) was performed and the results were compared

with numerical ones. From the results, the model showed to be efficiently and accurately enough to predicted the damage-dependent behavior of FAM.

To the end, with respect to the effect of replacing the hydrated lime filler by steel slag, it was found an increase in the material stiffness, which resulted in an earlier development of cohesive zone within the sample. However, damage propagation was slower for FAM_SS, resulting in higher fracture resistance. This behavior was observed both in the SCB fracture test, used for calibration of the NLVE-CZ fracture parameters and in the IDT used in the validation of the model. The analysis carried out about the fracture parameters was helpful to explain that influence.

In general, numerical analyzes results match well with the results found from laboratory tests, which in turn corroborate with the study of each fracture parameter influence on the mechanical behavior of the fine asphalt matrix (MAF). In other words, numerical model and its virtual tests can potentially replace expensive laboratory tests. In addition, there is a need for a better understanding of the NLVE-CZ parameters calibration to become the process of choosing the most efficient and precise parameter set.

The main advantage of using the microstructural numerical model in the evaluation of the performance of asphalt mixtures is that once you have an accurate numerical modeling approach, engineers could optimize mix design using much cheaper and faster numerical simulations, and then run laboratory experiments on the most promising optimized designs for verification before putting it in the field. In this way we have a significant savings in time, financial resources and human resources needed to laboratory performance tests to characterize damage in the mixtures. Another great advantage of using numerical modeling considering damage through cohesive zone models is the ability to investigate more explicitly the fracture phenomena, as it allows a more comprehensive examination of the

microstructural changes as damage evolves. Also, numerical simulations give more insight into the physical process governing material failure, because engineers can extract a lot more information, so that while in lab tests all one can get is the load curve and potentially some images, numerical simulations gives full range of variables (stress, strain, force, damage) to analyze.

Future Research Work

From the results and conclusions obtained in the present research it is suggested to future works:

- Using the model in two-way coupled multiscale computational analyses;
- Validate the model for other types of laboratory test conditions as well as for other type of composite media;
- Calibrate and Validate Mode II fracture parameters;
- Verify and calibrate the model for problems in three dimensions;
- Perform a rigorous study aiming a better understanding of the process of defining the set of fracture parameters with greater number and types of fracture tests.
- Trying different types of damages laws available in MultiMech;
- Using Nonlinear optimization tools to try to calibrate all damage parameters altogether.

REFERENCES

- ALFANO, G.; CRISFIELD, M. A. (2001) Finite element interface models for the delamination analysis of laminated composites: mechanical and computational issues. *International Journal for Numerical Method in Engineering*, 50, 1701–1736.
- ALLEN, D. H.; SEARCY, C. R. (2001) A micromechanical model for a viscoelastic cohesive zone. *International Journal of Fracture*, Vol. 107, p.159-176.
- ARAGÃO, F.T.S. (2011) **Computational Microstructure Modeling of Asphalt Mixtures Subjected to Rate-Dependent Fracture**. 140 f. PhD Thesis, The Graduate College at the University of Nebraska, University of Nebraska, Lincoln.
- ARAGÃO, F.T.S. and KIM, Y. (2012) Mode I fracture characterization of bituminous paving mixtures at intermediate service temperatures, *Exp. Mech.* 52 (9) 1423–1434.
- AASHTO TP 105-13. (2013) Standard Method of Test for Determining the Fracture Energy of Asphalt Mixtures Using the Semicircular Bend Geometry (SCB), American Association of State and Highway Transportation Officials.
- BAHIA, H. U. (1995) Critical evaluation of asphalt modification using strategic highway research program concepts. Washington: Transportation Research Record, n. 1488, p. 82-88.
- BAN, H., IM, S., KIM, Y. R. (2015) Mixed-mode fracture characterization of fine aggregate mixtures using semicircular bend fracture test and extended finite element modeling. *Construction and Building Materials* 101.
- BASHAM, K. D., CHONG, K. P., & BOSERI, A. P. (1990). A New Development in Devising Tension-Softening Curves for Brittle Materials. In *Proceedings of the Ninth International Conference on Experimental Mechanics*, Copenhagen, Denmark, 1423-1432.

BARENBLATT, G. I. (1962) The mathematical theory of equilibrium of cracks in brittle fracture. *Advances in Applied Mechanics*. Vol. 7. p. 55–129.

BERNUCCI, L. B.; MOTTA, L. M. G. DA; CERATTI, J. A. P.; SOARES, J. B. (2006) *Pavimentação Asfáltica. Formação Básica para Engenheiros*. Rio de Janeiro: Petrobras & ABEDA.

BERTHELOT, C.F.; ALLEN, D. H. ; SEARCY, C. R. (2003) Method for Performing Accelerated Characterization of Viscoelastic Constitutive Behavior of Asphaltic Concrete *Journal of Materials in Civil Engineering*, 15(5), p. 496-505.

CAMACHO, G. T.; ORTIZ, M. (1996) Computational Modeling of Impact Damage in Brittle Materials. *International Journal of Solid Structures*, Vol. 33, No. 20-22, pp. 2899-2938.

CAIAZZO, A. A.; COSTANZO, F. (2001) Modeling the Constitutive Behavior of Layered Composites with Evolving Cracks. *International Journal of Solids and Structures*, Vol. 38, p. 3469-3485.

CARNEIRO, F.L. (1943) Um novo método para determinação da resistência à tração dos concretos. Rio de Janeiro: Instituto Nacional de Tecnologia.

CASTELO BRANCO, V.T.F. (2004) **Caracterização de Misturas Asfálticas com o Uso de Escória de Aciaria como Agregado**. 153 f. Master Thesis, Universidade Federal do Rio de Janeiro (COPPE), Rio de Janeiro - RJ.

CASTELO BRANCO, V.T.F. (2008) **An Unified Method for the Analysis of Nonlinear Viscoelasticity and Fatigue Cracking of Asphalt Mixes Using the Dynamic Mechanical Analyzer**. PhD dissertation. Texas A&M University. College Station, TX.

CHANG, L.; KAIJIAN, N. (2013) Simulation of asphalt concrete cracking using Cohesive Zone Model. *Construction and Building Materials*. V. 38, p. 1097–1106.

CHEHAB, G.R., KIM, Y.R., SCHAPERLY, R.A., WITCZAK, M.W. e BONAQUIST, R. (2002) Time-Temperature Superposition Principle for Asphalt Concrete Mixtures with Growing Damage in Tension State. *Journal of the Association of Asphalt Paving Technologists*, Vol. 71.

CHRISTENSEN, R. M. (1982). *Theory of viscoelasticity: An introduction*. Academic, New York.

CNT- Confederação Nacional de Transportes. “Anuário CNT do Transporte – Estatísticas consolidadas”. Disponível em: < file:///C:/Users/Julia/Downloads/MaterialImprensa.pdf. > Acesso em: 07 de fevereiro 2017.

COUTINHO, R. P. (2012) **Utilização da parte fina de misturas asfálticas para avaliação do dano por fadiga**. 109 p. Master Thesis, Programa de Pós-Graduação em Engenharia de Transportes, Universidade Federal do Ceará (UFC), Fortaleza - CE.

COSME, R. L. (2015) **Estudo Reológico de Mástiques com Filer de Resíduo de Beneficiamento de Rochas Ornamentais (RBRO e Escória de Aciaria (EMA))**. Dissertação (Mestrado em Engenharia Civil). Programa de Pós Graduação em Engenharia Civil, Universidade Federal do Espírito Santo, Vitória.

COSME, R. L.; TEIXEIRA, J. E. S. L. (2016) Use of frequency sweep and MSCR tests to characterize asphalt mastics containing ornamental stone residues and LD steel slag. *Construction and Building Materials* 122, 556–566.

COSTANZO, F.; ALLEN, D. H. (1993). A Continuum Mechanics Approach to some Problems in Subcritical Crack Propagation. *International Journal of Fracture*, Vol. 63, pp. 27-57.

DANIEL, J.S.; KIM, Y.R. (2002). Development of a Simplified Fatigue Test and Analysis Procedure Using a Viscoelastic, Continuum Damage Model. *Journal of the Association of Asphalt Paving Technologists*, Vol. 71, p. 619-650.

DEALY, J. M. *Encyclopedia of Life Support System: Chemical Sciences, Engineering and Technology - Nonlinear Viscoelasticity*. Vol 1. Disponível em: [Disponível em: https://www.eolss.net/sample-chapters/C06/E6-197-06-00.pdf](https://www.eolss.net/sample-chapters/C06/E6-197-06-00.pdf)> Acesso em: 30 de abril 2018.

DIAO, J.; ZHOU, W.; KE, Z.; QIAO, Y.; ZHANG, T.; LIU, X.; XIE, B. (2016) System assessment of recycling of steel slag in converter steelmaking. *Journal of Cleaner Production*, Vol. 125, pp. 159 e 167.

DNER ME 043/95 – (1995a) Misturas betuminosas a quente - ensaio Marshall. DEPARTAMENTO NACIONAL DE ESTRADAS DE RODAGEM. Rio de Janeiro, RJ.

DNIT 136/2010 – ME (2010). Pavimentação asfáltica - Misturas asfálticas – Determinação da resistência à tração por compressão diametral – Método de ensaio. DEPARTAMENTO NACIONAL DE INFRAESTRUTURA DE TRANSPORTES, Rio de Janeiro, RJ.

DUGDALE, D.S. (1960) Yielding of steel sheets containing slits. *Journal of the Mechanics and Physics of Solids*. vol 8. p. 100–8.

EN 12697-44:2010 (2010). Bituminous Mixtures—Test Methods for Hot Mix Asphalt Part 44: Crack Propagation by Semi-Circular Bending Test, European Committee for Standardization, Brussels, Belgium.

ESPINOSA, H. D.; DWIVEDI, S.; LU, H. C. (2000) Modeling impact induced delamination of woven fiber reinforced composites with contact/cohesive laws. *Computer Methods in Applied Mechanics and Engineering*, 183 (3–4), 259–290.

ESPINOSA, H. D.; ZAVATTIERI, P. D. (2003) A grain level model for the study of failure initiation and evolution in polycrystalline brittle materials, part I: theory and numerical implementation. *Mechanics of Materials*, 35 (3–6), 333–364.

FONSECA, J.F. (2016) **Efeitos do Resíduo de Beneficiamento de Rochas Ornamentais e Escória de Aciaria como Fíleres na Rigidez Viscoelástica Linear e Características de Fratura da Matriz de Agregados Finos**. 122f. Master Thesis, Universidade Federal do Espírito Santo (UFES), Vitória - ES.

FREIRE, R. A.; BABADOPULOS, L. F. A. L.; CASTELO BRANCO, V. T. F. ; and BHASIN, A. (2017) Aggregate Maximum Nominal Sizes' Influence on Fatigue Damage Performance Using Different Scales. *Journal of Materials in Civil Engineering*, v29, inssue 8.

GEUBELLE, P. & BAYLOR, J. (1998). Impact-Induced Delamination of Laminated Composites: A 2D Simulation. *Composites Part B - Engineering*, 29 (5), 589-602.

GERDAU S.A. (2001). REGISTRATION STATEMENT PURSUANT TO SECTION 12(b) OR (g) OF THE SECURITIES EXCHANGE ACT OF 1934. Disponível em <http://www.gerdau.com.br/updatetool/DownloadCenter/_fls/_dwn/164_2.pdf>. Acesso 02/16/2018.

GOTTARDI, E. V. (2015). **Aproveitamento do Resíduo de Beneficiamento de Rochas Ornamentais e de Escória Moída de Aciaria como Filer em Pavimentos de Concreto Asfáltico**. 117f. Master Thesis, Universidade Federal do Espírito Santo (UFES), Vitória - ES.

GRIFFITH, A. A. (1920) The Phenomena of Rupture and flow in Solids. Philosophical Transactions of the Royal Society of London, Series A, Vol. 221, pp. 163-198.

HASSAN, N. A.; AIREY, G. D.; HAININ, M. R. (2014) Characterisation of micro-structural damage in asphalt mixtures using image analysis. Construction and Building Materials, s 54 27–38.

HELMS, K. L. E.; D. H. ALLEN e L. D. HURTADO (1999) A Model for Predicting Grain Boundary Cracking in Polycrystalline Viscoelastic Materials including Scale Effects. International Journal of Fracture, v. 95, p. 175-194.

IM, S., BAN, H. and KIM, Y. R. (2014) Characterization of mode-I and mode-II fracture properties of fine aggregate matrix using a semicircular specimen geometry. Construction and Building Materials 52 (2014) 413–421.

INSTITUTO AÇO BRASIL. (2015) Estatística Preliminar N°008. Rio de Janeiro. IRON AND STEEL. The Institute for Industrial Productivity. Disponível em: <<http://ietd.iipnetwork.org/content/iron-and-steel>>. Acesso em: 29 abril. 2018.

IRWIN, G. (1957) Analysis of stresses and strains near the end of a crack traversing a plate. Journal of Applied Mechanics 24, 361–364.

KACHANOV, L.M. (1958). On the creep fracture time. Izv. Acad. Nauk SSSR Otd. Tekhn. 8, 26–31.

KARKI, P. (2010). **Computational and Experimental Characterization of bituminous Composites based on Experimentally Determined Properties of Constituents.** Master Thesis, University of Nebraska–Lincoln.

KHALID, H. A. & ARTAMENDI, I. (2008). Measurement and Effective Evaluation of Crack Growth in Asphalt Mixtures. *Pavement Cracking: Mechanisms, Modeling, Detection, Testing, and Case Histories*, edited by I. L. Al-Qadi, T. Scarpas, and A. Loizos, CRC Press, 417-425.

KLEIN, P., et al. (2001) Physics-based modeling of brittle fracture: cohesive formulations and the application of mesh-free methods. Technical Report SAND2001-8099, Sandia National Laboratories.

KIM, Y-R. (2003) **Mechanistic Fatigue Characterization and Damage Modeling of Asphalt Mixtures.** Ph.D. Dissertation, Texas A&M University, College Station, EUA.

KIM, Y. R (2011) Cohesive Zone Model to Predict Fracture in Bituminous Materials and Asphaltic Pavements: State-of-the-Art Review. *International Journal of Pavement Engineering* 12:4, pp. 343–356.

KIM, Y.-R., ARAGÃO, F.T.S. (2013) Microstructure modeling of rate-dependent fracture behavior in bituminous paving mixtures. *Fin. Elem. Analyses and Design* 63, 23–32.

LEE, H. J.; KIM, Y. R. (1998) Viscoelastic Continuum Damage Model of Asphalt Concrete with Healing. *Journal of Engineering Mechanics*, Vol. 124, n.11, p. 1224-1232.

LI, X. & MARASTEANU, M. O. (2004). Evaluation of the Low Temperature Fracture Resistance of Asphalt Mixtures Using the Semi Circular Bend Test. *Journal of the Association of Asphalt Paving Technologists*, 73, 401-426.

LI, X. & MARASTEANU, M. O. (2010). Using Semi Circular Bending Test to Evaluate Low Temperature Fracture Resistance for Asphalt Concrete. *Experimental Mechanics*, 50, 867-876.

LITTLE, D. N., J. A. (2006) Epps, and Sebaaly, P. E. The benefits of hydrated lime in hot mix asphalt. Report by National Lime Association.

LUTIF, J. E. S. (2011) **Computational micromechanics modeling of damage-dependent bituminous composites based on two-way coupled multiscale approach**. 139 f. PhD Thesis, The Graduate College at the University of Nebraska, University of Nebraska, Lincoln.

MAHIEUX, P.Y.; AUBERT, J.E.; ESCADEILLAS G. (2008) Utilization of weathered basic oxygen furnace slag in the production of hydraulic road binders. *Construction and Building Materials*. 23:742–7

MOHAMMED, I. & LIECHTI, K. (2000). Cohesive Zone Modeling of Crack Nucleation at Bimaterial Corners. *Journal of the Mechanics and Physics of Solids*, 48, 735-764.

MONSHI, A.; ASGARANI, M. K. (1999) Producing Portland cement from iron and steel slags and limestone. *Cement And Concrete Research*.

MULTIMECH TM SOFTWARE. Available in: < <http://multimechanics.com/>> accessed in: August 1, 2018.

NEEDLEMAN, A. (1987). A Continuum Model for Void Nucleation by Inclusion Debonding. *Journal of Applied Mechanics*, Vol. 54, pp. 525-531.

NEEDLEMAN, A. (1990a). An Analysis of Decohesion Along an Imperfect Interface. *International Journal of Fracture*, 42, 21–40.

NEEDLEMAN, A. (1990b). An Analysis of Tensile Decohesion Along an Interface. *Journal of Mechanics and Physics of Solids*, 38 (3), 289-324.

PARK, S. W.; KIM, Y. R.; SCHAPERLY, R. A. (1996) A Viscoelastic Continuum Damage Model and its Application to Uniaxial Behavior of Asphalt Concrete. *Mechanics of Materials*, Vol. 24, n.4, p. 241-255.

PHILLIPS, M. L.; C. YOON e D. H. ALLEN (1999) A Computational Model for Predicting Damage Evolution in Laminated Composite Plates. *Journal of Engineering Materials and Technology*, v. 121, p. 436-444.

RABOTNOV, Y. N. (1969). *Creep Problems in Structural Members*. North-Holland, London.

SCHAPERLY, R. A. (1962). Approximate Methods of Transform Inversion for Viscoelastic Stress Analysis. *Proc. 4th U. S. Nat. Cong. Appl. Mech.*, 1075.

SCHAPERLY, R. A. (1975). A Theory of crack Initiation and Growth in Viscoelastic Media; Part I: Theoretical Development". *International Journal of Fracture*, Vol. 11, n.1, pp. 141-159.

SCHAPERLY, R. A. (1990) Simplifications in the Behavior of Viscoelastic Composites with Growing Damage. *Proceedings of the IUTAM Symposium in Inelastic Deformation of Composite Materials*, troy, New York, p. 193-214.

SEIDEL ,G. D.; ALLEN, D. H.; HELMS K. L. E.;and GROVES, S. E.. (2005) A model for predicting the evolution of damage in viscoelastic particle-reinforced composites. *Mechanics of Materials*, 37(1):163-178.

SHI, C. (2004) Steel Slag—Its Production, Processing, Characteristics, and Cementitious Properties. *Journal of Materials in Civil Engineering*, Vol. 16, p 230-236.

SONG, S.H.; PAULINO, G.H.; BUTTLAR, W.G. (2006) A bilinear cohesive zone model tailored for fracture of asphalt concrete considering viscoelastic bulk material, *Eng. Fracture Mech.* 73, 2829–2847.

SOUZA, F. V.; J. B. SOARES; D. H. ALLEN e F. EVANGELISTA JR. (2004) Model for Predicting Damage Evolution in Heterogeneous Viscoelastic Asphaltic Mixtures. A ser publicado em *Transportation Research Record*, Transportation Research Board, National Research Council, EUA.

SOUZA, F. V. (2005) **Modelo multi-escala para análise estrutural de compósitos viscoelásticos suscetíveis ao dano.** 198 f. Dissertação (Mestrado em Engenharia de Transportes) – Programa de Mestrado em Engenharia de Transportes, Universidade Federal do Ceará (UFC), Fortaleza - CE.

TEIXEIRA, V. F.; SOUZA, F. V.; SOARES, J. B. (2007) Modelagem da vida de fadiga e do acúmulo de deformações permanentes em pavimentos asfálticos por meio de um modelo de dano contínuo. *TRANSPORTES*, Vol. XV, n. 2, p. 17-25.

TEIXEIRA, J. E. S. L.; KIM, Y. R.; SOUZA, F. V.; ALLEN, D. H.; LITTLE, D. N. (2014) A Multiscale Model for Asphalt Mixtures Subjected to Cracking and Viscoelastic Deformation. *Transportation Research Record*, v. 2447, p. 136-145.

TUAN NGUYEN, M.; LEE, H. J.; and BAEK, J., (2013) Fatigue Analysis of Asphalt Concrete under Indirect Tensile Mode of Loading Using Crack Images. *Journal of Testing and Evaluation*, Vol. 41, No. 1, pp. 1–11.

TSAKIRDIS, P.E.; PAPADIMITRIOU, G.D.; TSIVILIS, S.; KORONEOS, C. (2007) Utilization of steel slag for Portland cement clinker production. *Journal of Hazardous Materials.* 152:805–11.

TVERGAARD, V. (1990) Effect of Fiber Debonding in a Whisker-Reinforced Metal. *Materials Science and Engineering*, Vol. A125, n. 2, pp. 203-213.

UNDERWOOD, B. S.; KIM, Y. R. , P.E. (2013) Microstructural Association Model for Upscaling Prediction of Asphalt Concrete Dynamic Modulus. *Journal of Materials in Civil Engineering*, 25(9), p. 1153-1161.

VAN ROOIJEN, R. C. & de BONDT, A. H. (2008). Crack Propagation Performance Evaluation of Asphaltic Mixes Using a New Procedure Based on Cyclic Semi-Circular Bending Tests. *Pavement Cracking: Mechanisms, Modeling, Detection, Testing, and Case Histories*, edited by I. L. Al-Qadi, T. Scarpas, and A. Loizos, CRC Press, 437-446.

VOYIADJIS, G. Z; KATTAN, P. I. (2012). A New Class of Damage Variables in Continuum Damage Mechanics. *Journal Eng. Mater. Technol* 134(2).

XU, X. P. & NEEDLEMAN, A. (1994). Numerical Simulation of Fast Crack Growth in Brittle Solids. *Journal of Mechanics and Physics of Solids*, 42 (9), 1397-1434.

YOON, C.; ALLEN, D. H. (1999). Damage Dependent Constitutive Behavior and Energy Release Rate for a Cohesive Zone in a Thermoviscoelastic Solid. *International Journal of Fracture*, 96, 55-74.

YOON, H. H, and TARRER, A. R. (1988) Effect of Aggregate Properties on Stripping. In *Transportation Research 42 Record: Journal of the Transportation Research Board*, No. 1171, 1988, pp. 37-43.

WORLD STEEL ASSOCIATION (2017) *World Steel in Figures 2017*. Belgium.

ZAVATTIERI, P. D.; ESPINOSA, H. D. (2001) Grain level analysis of crack initiation and propagation in brittle materials. *Acta Materialia*, 49 (20), 4291–4311.